NASA TECHNICAL NOTE

NASA TN D-6220

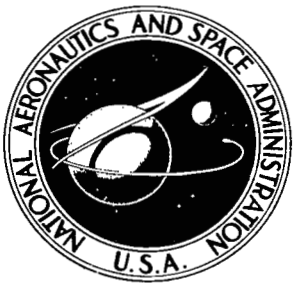

NASA TN D-6220

c 1

LOAN COPY: RETUR
AFWL (DOGL)
KIRTLAND AFB, N

TECH LIBRARY KAFB, NM

NUMERICAL ANALYSIS OF THE TRANSIENT RESPONSE OF ABLATING AXISYMMETRIC BODIES INCLUDING THE EFFECTS OF SHAPE CHANGE

by Stephen S. Tompkins, James N. Moss, Claud M. Pittman, and Lona M. Howser

Langley Research Center
Hampton, Va. 23365

NATIONAL AERONAUTICS AND SPACE ADMINISTRATION • WASHINGTON, D. C. • MAY 1971

TECH LIBRARY KAFB, NM
0133002

1. Report No.	2. Government Accession No.	3. Recipient's Catalog No.
NASA TN D-6220		

4. Title and Subtitle	5. Report Date
NUMERICAL ANALYSIS OF THE TRANSIENT RESPONSE OF ABLATING AXISYMMETRIC BODIES INCLUDING THE EFFECTS OF SHAPE CHANGE	May 1971
	6. Performing Organization Code
7. Author(s)	8. Performing Organization Report No.
Stephen S. Tompkins, James N. Moss, Claud M. Pittman, and Lona M. Howser	L-7474
	10. Work Unit No.
9. Performing Organization Name and Address	124-07-26-02
NASA Langley Research Center Hampton, Va. 23365	11. Contract or Grant No.
	13. Type of Report and Period Covered
12. Sponsoring Agency Name and Address	Technical Note
National Aeronautics and Space Administration Washington, D.C. 20546	14. Sponsoring Agency Code

15. Supplementary Notes

16. Abstract

The differential equations governing the transient response of an ablating axisymmetric, orthotropic body have been derived for fixed points in a moving coordinate system. These equations have been expanded into finite-difference form and programed for numerical solution, with an implicit technique, on a digital computer. Numerical results compare favorably with exact solutions.

Several applications of the analysis are discussed. These applications demonstrate the significance of a salient feature of the analysis, that is, the ability to analyze the effects of changes in body geometry. This feature was used to obtain satisfactory agreement between numerical and experimental results for an ablating teflon sphere and a small test specimen exposed to a high-intensity laser beam. Although the analysis is primarily for a single-layer material, a multilayer material can be successfully approximated under certain conditions by a single-layer system.

17. Key Words (Suggested by Author(s))	18. Distribution Statement
Ablation Heat transfer Numerical analysis	Unclassified – Unlimited

19. Security Classif. (of this report)	20. Security Classif. (of this page)	21. No. of Pages	22. Price*
Unclassified	Unclassified	43	$3.00

*For sale by the National Technical Information Service, Springfield, Virginia 22151

NUMERICAL ANALYSIS OF THE TRANSIENT RESPONSE OF ABLATING AXISYMMETRIC BODIES INCLUDING THE EFFECTS OF SHAPE CHANGE

By Stephen S. Tompkins, James N. Moss, Claud M. Pittman,
and Lona M. Howser
Langley Research Center

SUMMARY

The differential equations governing the transient response of an ablating axisymmetric, orthotropic body have been derived for fixed points in a moving coordinate system. These equations have been expanded into finite-difference form and programed for numerical solution, with an implicit technique, on a digital computer. Numerical results compare favorably with exact solutions.

Several applications of the analysis are discussed. These applications demonstrate the significance of a salient feature of the analysis, that is, the ability to analyze the effects of changes in body geometry. This feature was used to obtain satisfactory agreement between numerical and experimental results for an ablating teflon sphere and a small test specimen exposed to a high-intensity laser beam. Although the analysis is primarily for a single-layer material, a multilayer material can be successfully approximated under certain conditions by a single-layer system.

INTRODUCTION

One-dimensional ablation analyses have been used extensively to study the thermal response of heat shields subjected to aerodynamic heating. However, for heat shields with large curvature or large heating-rate variations over the surface, the assumptions of one-dimensional heat flow no longer apply, and an accurate description of the thermal response requires an ablation analysis for multidimensional heat transfer that includes the effects of changes in heat-shield geometry.

References 1 to 6 are examples of two-dimensional thermal analyses presently available. The outstanding features of the analyses of references 1 and 2 are that both consider axisymmetric bodies of anisotropic materials and both use stable, implicit numerical methods to solve the heat-conduction equation. However, neither analysis considers mass transfer. Mass transfer is included in the analysis of reference 3 in

addition to the indicated features of references 1 and 2. The analysis of reference 3 is formulated for fixed nodal points in a fixed coordinate system and often requires interpolation at the boundaries because the nodal points and the boundaries do not always coincide. This interpolation can lead to inaccuracies. The analysis of reference 4 is similar to that of reference 3 except that it uses a moving coordinate system (which eliminates interpolation) and a conditionally stable, time-consuming explicit formulation as opposed to the stable, time-saving implicit formulation used in references 1 to 3. Only references 5 and 6 consider the effects of shape change on the thermal response of the heat shield. However, reference 5 does not consider an anisotropic material, and both references 5 and 6 use explicit methods to solve the governing equations.

Collectively, references 1 to 6 consider many of the significant physical characteristics of an axisymmetric ablating heat shield and also demonstrate the desirable method of solution, that is, an implicit method. However, no single reference incorporates all these features into one analysis.

This paper presents and discusses a transient two-dimensional ablation analysis which incorporates all the significant characteristics of the physical problem considered collectively in references 1 to 6. The analysis has the following features: (1) the ablation material is considered to be orthotropic with temperature-dependent thermal properties; (2) the thermal response of the entire body is considered simultaneously; (3) the heat-transfer and pressure distribution over the body are adjusted to the new geometry as ablation occurs; (4) the governing equations and several boundary-condition options are formulated in terms of generalized orthogonal coordinates for fixed points in a moving coordinate system; and (5) the finite-difference equations are derived and solved implicitly.

The accuracy of the analysis presented in this paper is demonstrated by comparisons between numerical results and exact solutions for simplified conduction problems. Selected examples and test data are shown to demonstrate the utility of the analysis and the importance of the coupling between body-shape change and the heating-rate and pressure distributions.

The finite-difference equations have been programed for solution on a high-speed digital computer. The program has a plotting routine which can display the shape of the ablating body at any time during the calculation.

SYMBOLS

$A = \frac{1}{x_b}\frac{\partial \delta}{\partial \xi}$ defined by equation (10)

A_c constant in oxidation equation corresponding to specific reaction rate

A_j, B_j, C_j, D_j	coefficients in equation (28)
A_s	constant in sublimation equation
a	constant to adjust equations (C24), (C25), and (C26) to correct form for Cartesian coordinates
$B = h_1 h_3 k$	
B_c	constant in exponential of oxidation equation corresponding to activation energy
B_s	constant in exponential of sublimation equation
C	oxygen concentration by mass
c_p	specific heat
H	total enthalpy
ΔH_c	heat of combustion
ΔH_s	heat of sublimation
h_1, h_2, h_3	coordinate scale factors (eqs. (2))
i	order of reaction (eq. (11))
K	reaction-rate constant for oxidation (eq. (15))
k	thermal conductivity
L	number of stations in x-direction
M	molecular weight of gas
M_{O_2}	molecular weight of oxygen

m,n	integers
$\dot{m}$	mass loss rate
$\dot{m}_{O_2}$	rate at which oxygen diffuses to surface
$\dot{m}_s$	mass loss due to sublimation
p	exponent of pressure in sublimation equation (eq. (17))
p_w	wall pressure
q_C	convective heating rate to nonablating cold wall
$q_{C,net}$	hot-wall convective heating rate corrected for transpiration (eq. (13))
q_{net}	net heating rate to surface including combustion, sublimation, and surface reradiation (eq. (19))
q_r	radiant heating rate
R	radius of curvature of base curve
R_{cyl}	cylindrical radius from axis of symmetry to base curve
R_{stag}	stagnation-point radius of curvature
r	exponent of radius in sublimation equation (17); spherical coordinate
S	number of stations in y-direction
T	temperature
T_B	temperature of body to which back surface radiates
$T_{m,n}$	temperature at finite-difference station (m,n)
t	thickness of heat sink

U_∞	free-stream velocity
w,z	Cartesian coordinates (see fig. 2)
x,y	curvilinear coordinates (see fig. 1)
x_b	length of base curve
α	absorptance
α_c	weighting factor for transpiration effectiveness of mass loss due to combustion
α_s	weighting factor for transpiration effectiveness of mass loss due to sublimation
β	either 0 or 1 depending on whether transpiration or ablation theory is used
δ	material thickness
ϵ	emittance
θ	angle between R and R_{cyl} (fig. 1); spherical coordinate
λ	mass of char removed per unit mass of oxygen
ξ,η	dimensionless curvilinear coordinates, equations (4)
ρ	density of material
σ	Stefan-Boltzmann constant
τ	time
φ	angle of rotation about axis of symmetry, figure 3
ψ	angle between axis of symmetry and normal to surface, figure 1

Subscripts:

c	combustion
e	edge of boundary layer
m,n	integers
L	last station in x-direction
max	maximum
o	original, value at previous time
S	last station in y-direction
stag	stagnation-point condition
w	wall condition
x,y	coordinates
ξ,η	dimensionless coordinates

Superscripts:

'	condition along $x = L$
''	condition along $y = 0$

ANALYSIS

Physical Model

The analysis considers an axisymmetric ablating body exposed to aerodynamic heating; this body is composed of a single orthotropic material of varying thickness with temperature-dependent thermal properties. (See fig. 1.) Although the analysis considers a single-layer material, the analysis of a multilayer material, such as a charring ablator, can be successfully approximated with the present analysis under certain conditions. (See ref. 7, for example.)

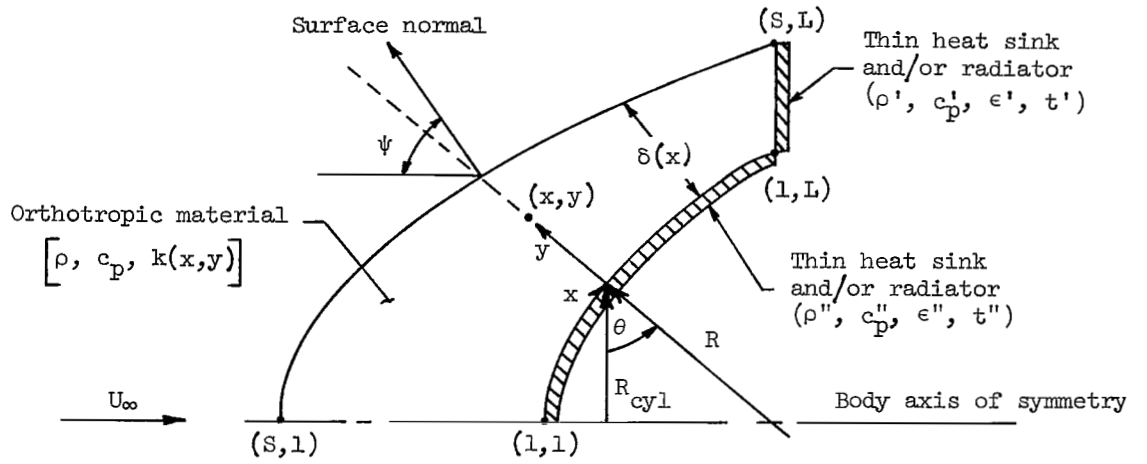

Figure 1.- Schematic diagram of the physical model for a typical axisymmetric body.

Two coordinate systems are used to study the thermal and ablative response of the heat shield. One is a curvilinear coordinate system with x,y coordinates (fig. 1), which is used to determine internal temperature distributions. A stationary base curve located at the back surface of the ablator establishes the x-axis.

The second coordinate system (fig. 2) is used to define the heat-shield exterior

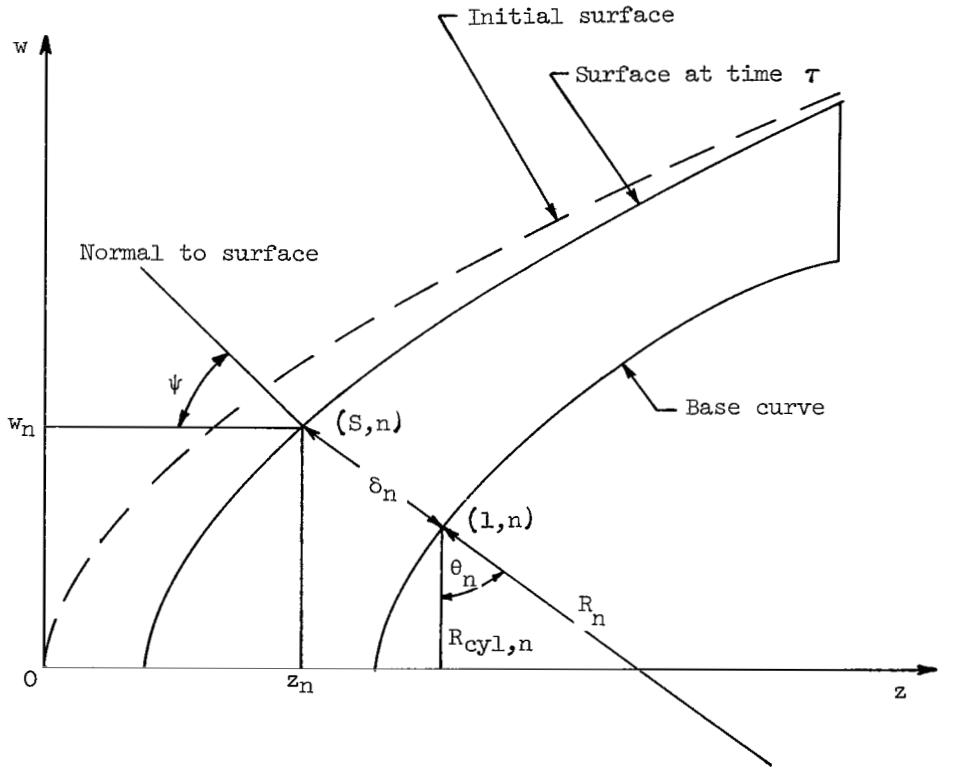

Figure 2.- Coordinate system used to define body geometry.

geometry which changes with time as a result of ablation. This coordinate system, with w,z coordinates, is a Cartesian system with the origin fixed at the original stagnation point on the heat shield. All the geometric parameters needed to compute changes in the stagnation heating rates and the heating-rate and pressure distributions over the surface are defined in this system. The equations that quantitatively relate the internal temperatures with the changes in the heating and pressure over the surface of the heat shield are given in the following sections.

Governing Differential Equations

The differential arc length ds in the curvilinear coordinate system in figure 3 is

$$(ds)^2 = h_1^2(dx)^2 + h_2(dy)^2 + h_3(d\varphi)^2 \tag{1}$$

where the scale factors are

$$h_1 = 1 + \frac{y}{R} \tag{2a}$$

$$h_2 = 1 \tag{2b}$$

$$h_3 = R_{cyl} + y \cos \theta \tag{2c}$$

The curvilinear coordinate system should conveniently describe any axisymmetric body geometry of interest. However, if the Cartesian coordinate system is required, care must be taken to use unity scale factors. Unity scale factors are obtained by assigning the values of 1 to R_{cyl}, ∞ to R, and $\pi/2$ to θ. (See eqs. (2).)

For an axisymmetric body, the governing time-dependent heat-conduction equation with variable coefficients is (in fixed coordinates)

$$\frac{1}{h_1 h_2 h_3}\left[\frac{\partial}{\partial x}\left(\frac{h_2 h_3}{h_1} k_x \frac{\partial T}{\partial x}\right) + \frac{\partial}{\partial y}\left(\frac{h_1 h_3}{h_2} k_y \frac{\partial T}{\partial y}\right)\right] = \rho c_p \frac{\partial T}{\partial \tau} \tag{3}$$

If equation (3) were expressed in finite-difference form, it would describe the temperature variation at fixed stations in a fixed coordinate system. To maintain a fixed number of stations in a layer which changes thickness with time, it is necessary to change the locations of the stations and to interpolate to determine the temperatures at the new location after each time step in the calculation. This procedure not only increases the time required to perform the computations but also introduces a small error in each step of the calculation. An alternative to this procedure is to transform

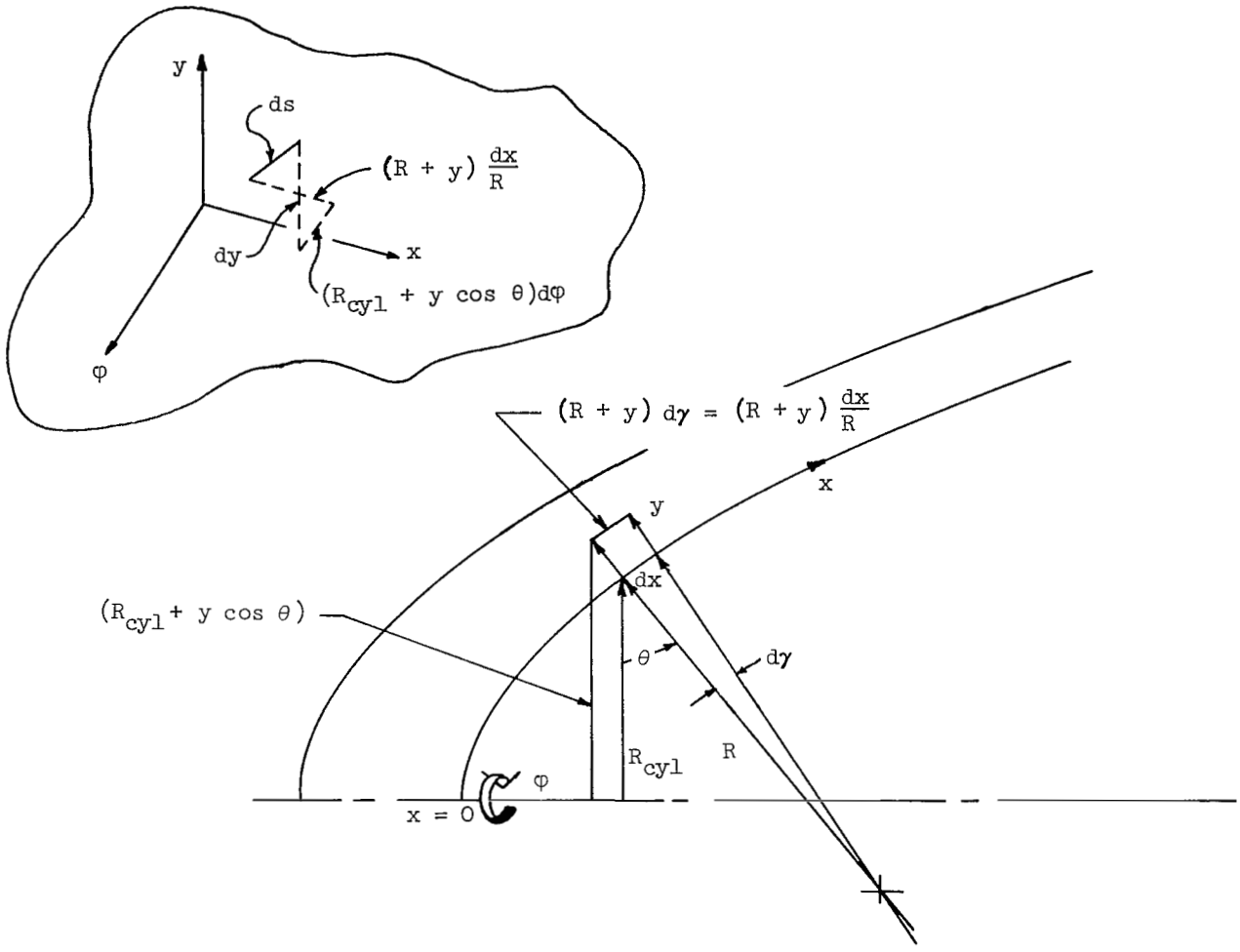

Figure 3.- Basic curvilinear coordinate system.

the equation to a coordinate system in which the stations remain fixed and the coordinates themselves move to accommodate changes in the surface location.

This transformation can be made by introducing a moving coordinate system which is defined by the following relations:

$$\xi = \frac{x}{x_b} \qquad \text{and} \qquad \eta = \frac{y}{\delta} \tag{4}$$

In this system, the outer surface remains fixed at $\eta = 1$ and all other stations remain at fixed values of η.

Before equation (3) can be transformed to the ξ,η coordinates, derivatives with respect to x and y in terms of ξ and η must be determined. These derivatives are given in the following equations:

$$\frac{D}{\partial x} = \frac{\partial \xi}{\partial x}\frac{\partial}{\partial \xi} + \frac{\partial \eta}{\partial x}\frac{\partial}{\partial \eta} = \frac{1}{x_b}\frac{\partial}{\partial \xi} - \frac{\eta}{\delta}\frac{\partial \delta}{\partial x}\frac{\partial}{\partial \eta} \tag{5}$$

and

$$\frac{D}{\partial y} = \frac{\partial \xi}{\partial y}\frac{\partial}{\partial \xi} + \frac{\partial \eta}{\partial y}\frac{\partial}{\partial \eta} = \frac{1}{\delta}\frac{\partial}{\partial \eta} \tag{6}$$

Because η is a function of δ which is also a function of time, the time derivative on the right side of equation (3) becomes

$$\frac{D}{\partial \tau} = \frac{\partial \xi}{\partial \tau}\frac{\partial}{\partial \xi} + \frac{\partial \eta}{\partial \tau}\frac{\partial}{\partial \eta} + \frac{\partial}{\partial \tau} \tag{7a}$$

The derivatives of ξ and η are, from equations (4),

$$\left.\begin{aligned} \frac{\partial \xi}{\partial \tau} &= \frac{1}{x_b}\frac{\partial x}{\partial \tau} = 0 \\ \frac{\partial \eta}{\partial \tau} &= \frac{\partial \eta}{\partial \delta}\frac{\partial \delta}{\partial \tau} = -\frac{\eta}{\delta}\frac{\partial \delta}{\partial \tau} \end{aligned}\right\} \tag{7b}$$

A change in δ is given by

$$\delta - \delta_o = -\int \frac{\dot{m}}{\rho}\, d\tau \tag{7c}$$

Therefore,

$$\frac{\partial \delta}{\partial \tau} = -\frac{\dot{m}}{\rho} \tag{7d}$$

Replacing the appropriate terms in equation (7a) with equations (7b) and (7d) gives

$$\frac{D}{\partial \tau} = \frac{\partial}{\partial \tau} + \frac{\eta}{\delta}\frac{\dot{m}}{\rho}\frac{\partial}{\partial \eta} \tag{8}$$

Substituting equations (2b), (5), (6), and (8) into equation (3) gives, in the transformed moving coordinates,

$$\frac{1}{h_1 h_3}\left[\frac{1}{\delta^2}\frac{\partial}{\partial \eta}\left(h_1 h_3 k_\eta \frac{\partial T}{\partial \eta}\right) + \frac{1}{x_b^2}\frac{\partial}{\partial \xi}\left(\frac{h_3}{h_1} k_\xi \frac{\partial T}{\partial \xi}\right) - \frac{1}{x_b}\frac{\partial}{\partial \xi}\left(\frac{h_3}{h_1} k_\xi \frac{\eta A}{\delta}\frac{\partial T}{\partial \eta}\right) - \frac{\eta A k_\xi}{\delta x_b}\frac{\partial}{\partial \eta}\left(\frac{h_3}{h_1}\frac{\partial T}{\partial \xi}\right)\right.$$

$$\left. + \frac{\eta A}{\delta^2} k_\xi \frac{\partial}{\partial \eta}\left(\frac{h_3}{h_1}\eta A \frac{\partial T}{\partial \eta}\right)\right] = \rho c_p\left(\frac{\partial T}{\partial \tau} + \frac{\dot{m}\eta}{\rho\delta}\frac{\partial T}{\partial \eta}\right) \tag{9}$$

where

$$A = \frac{1}{x_b}\frac{\partial \delta}{\partial \xi} \tag{10}$$

The solution to equation (9) depends on the initial conditions and the specified boundary conditions. These conditions are discussed in the following sections.

Initial Conditions

The initial conditions that must be specified are the temperature distribution, mass-transfer rates, and the body shape. For most cases of interest, the initial temperature distribution is uniform and the initial mass-transfer rate is zero.

Surface Boundary Conditions

Two conditions must be specified at the outer surface. Either the rate of removal of the surface material or the surface temperature must be specified; the other condition is provided by an energy balance at the surface.

Surface recession.- Ablation is assumed to result from a chemical process (oxidation) or from a phase-change process (sublimation). The rate of mass loss due to oxidation by molecular oxygen is, for an ith-order reaction,

$$\dot{m}_c = A_c\left(C_w p_w \frac{M_w}{M_{O_2}}\right)^i e^{-B_c/T_w} \tag{11}$$

In this analysis, it is assumed that all oxygen at the surface is in molecular form.

The net rate at which oxygen diffuses to the surface is, from reference 8 (assuming a unit Lewis number),

$$\dot{m}_{O_2} = \frac{q_{C,net}}{H_e - H_w}\left(C_e - C_w\right) \tag{12}$$

where

$$q_{C,net} = q_C\left(1 - \frac{H_w}{H_e}\right)\left\{1 - (1-\beta)\left[0.6\,\frac{H_e}{q_C}\left(\alpha_c\dot{m}_c + \alpha_s\dot{m}_s\right) - 0.084\left(\frac{H_e}{q_C}\right)^2\left(\alpha_c\dot{m}_c + \alpha_s\dot{m}_s\right)^2\right]\right.$$
$$\left. - \beta\left(\alpha_c\dot{m}_c + \alpha_s\dot{m}_s\right)\left(\frac{H_e}{q_C}\right)\right\} \tag{13}$$

which is the net convective heating rate to a hot ablating surface. Either transpiration theory ($\beta = 0$) or linear ablation theory ($\beta = 1$) can be used to account for the effects of mass transfer on the convective heating rate.

The rate at which mass is removed by oxygen must be proportional to the net rate at which oxygen diffuses to the surface; that is,

$$\dot{m}_C = \lambda \dot{m}_{O_2} \tag{14}$$

Therefore, combining equations (11), (12), and (14) gives the rate of ablation by oxidation in a half-order reaction $\left(i = \frac{1}{2}\right)$ as

$$\dot{m}_C = \frac{1}{2}\left\{ - \frac{M_W(H_e - H_W)K^2 p_W}{M_{O_2} q_{C,net} \lambda} + \sqrt{\left[\frac{M_W(H_e - H_W)K^2 p_W}{M_{O_2} q_{C,net} \lambda}\right]^2 + 4K^2 C_e \frac{M_W}{M_{O_2}} p_W} \right\} \tag{15}$$

where

$$K = A_c e^{-B_c/T_W}$$

The equation for a first-order oxidation reaction (i = 1) is

$$\dot{m}_C = \frac{K p_W C_e}{\frac{M_{O_2}}{M_W} + \frac{K p_W (H_e - H_W)}{q_{C,net} \lambda}} \tag{16}$$

Equations (15) and (16) apply to both the reaction-rate-controlled and the diffusion-controlled oxidation regimes as well as the intermediate conditions.

The rate of ablation by sublimation is

$$\dot{m}_S = \frac{A_S (p_W)^p}{(R_{stag})^r} e^{-B_S/T_W} \tag{17}$$

The form of equation (17) is compatible with reference 9 and most other sublimation theories. Either equation (15), (16), or (17) can be the boundary condition that defines the rate of removal of the surface material.

Surface location.- The thickness at any point ξ at any time is

$$\delta = \delta_o - \int_0^\tau \frac{\dot{m}}{\rho} d\tau \tag{18}$$

The mass-loss variation about the body caused by the heating-rate distribution will result in a nonuniform change in the geometry of the outer surface. This effect will in turn affect the heating and pressure distribution as discussed in a subsequent section.

Surface energy balance.- The heat input to the surface consists of convective and radiative heating and heat from combustion when oxidation occurs. This heat input must be accommodated by one or more of the following mechanisms: (1) aerodynamic blocking by mass transfer, (2) reradiation from the surface, (3) conduction into the material, and (4) sublimation of the surface material.

The surface energy balance is

$$q_{net} = \frac{k_\eta}{\delta} \frac{\partial T}{\partial \eta} \tag{19}$$

where

$$q_{net} = q_{C,net} + \alpha q_r + \dot{m}_c \Delta H_c - \dot{m}_s \Delta H_s - \sigma \epsilon T_w^4 \tag{20}$$

The heat absorbed during sublimation and the heat released during oxidation are considered separately in equation (20) as is the blocking effectiveness of the gases produced by oxidation and sublimation in equation (13). In the present analysis, oxidation and sublimation are not allowed to occur simultaneously.

The mass transfer affects only convective heating in this analysis. Reference 10 indicates that at hypersonic entry velocities, radiant heating may also be significantly affected by mass transfer. However, at present there is no quantitative analysis for the effect of mass transfer on radiant heating, and it is therefore neglected. Additional terms can easily be included in equation (20) to account for other phenomena which may affect the energy input to the surface.

Correction for change in body geometry.- The heat input to the surface is also affected by changes in body geometry. In the present analysis, the stagnation convective and radiative heat-transfer rates are adjusted for changes in the body bluntness as follows:

$$q_C = q_{C,o} \frac{\sqrt{R_{stag,o}}}{\sqrt{R_{stag}}} \qquad \text{and} \qquad q_r = q_{r,o} \frac{R_{stag,o}}{R_{stag}} \tag{21}$$

Geometry changes affect the heating and pressure distribution around the body as well. The heating-rate distribution is computed by using equation (14) of reference 11 and modified Newtonian pressure distribution. The methods for evaluating the body shape parameters which are used to determine the heating-rate and pressure distributions are given in appendix A.

Modified Newtonian pressure distributions are sufficiently accurate for most applications where the body is a hemisphere or a hemispherically blunted cone. For cones, the cone angle must be less than the value required to maintain supersonic flow over the conical portion of the body. Also, for ablating hemispherical or hemispherically capped bodies, the modified Newtonian pressure distribution and consequently the heating-rate distributions become inaccurate as the body shapes are blunted; that is, as the ratio of the body radius to nose radius approaches zero.

Boundary Conditions Along the ξ-Axis ($0 \leqq \xi \leqq 1$, $\eta = 0$)

Several options or combinations of conditions are considered along the surface $\eta = 0$ ($y = 0$). This interior surface may be perfectly insulated or lined with a heat sink which may or may not radiate energy to a body at a constant temperature T_B. The boundary condition is

$$\frac{k_y}{\delta}\frac{\partial T}{\partial \eta} = c_p''\rho''t''\frac{\partial T}{\partial \tau} + \sigma\epsilon''\left(T^4 - T_B^4\right) \tag{22}$$

The layer along $\eta = 0$ is assumed to have a constant heat capacity $\rho''c_p''t''$.

Boundary Conditions Along $\xi = 1$, $0 \leqq \eta \leqq 1$

The same conditions may exist along this surface that exist along $\eta = 0$, $0 \leqq \xi \leqq 1$. The boundary condition along this surface is

$$\frac{k_x}{h_1}\frac{DT}{\partial x} = -\rho'c_p't'\frac{\partial T}{\partial \tau} - \sigma\epsilon'\left(T^4 - T_B^4\right) \tag{23}$$

The thermally thin layer along $\xi = 1$ is assumed to have a constant heat capacity $\rho'c_p't'$.

Boundary Conditions Along Line of Symmetry ($\xi = 0$, $0 < \eta < 1$)

The assumption of an axisymmetric body requires the following boundary conditions along the line of symmetry:

$$\frac{DT}{\partial x} = \frac{1}{x_b}\frac{\partial T}{\partial \delta} - \frac{\eta A}{\delta}\frac{\partial T}{\partial \eta} = 0 \tag{24a}$$

and

$$A = \frac{1}{x_b}\frac{\partial \delta}{\partial \xi} = 0 \tag{24b}$$

The boundary conditions along this line of symmetry at the surface $\xi = 0$, $\eta = 1$ and at $\eta = 0$ are the same as those previously described. However, this line is mathematically a singularity for equation (3). The equations required along this line are discussed in the following section.

Singularities

Equation (3) applies to the entire region of interest; however, a line of discontinuity (singularity) exists. An inspection of equation (2c) shows that at $x = 0$, that is, along the line of symmetry, the scale factor h_3 vanishes. This coordinate singularity can be eliminated by using proper approximations valid only near $x = 0$. Appendix B presents a detailed derivation of a form of equation (3) that applies at $x = 0$ and is given in ξ,η coordinates as

$$\frac{2k_\xi}{h_1^2}\left(\frac{1}{x_b^2}\frac{\partial^2 T}{\partial \xi^2} - \frac{1}{x_b}\frac{\eta}{\delta}\frac{\partial T}{\partial \eta}\frac{\partial A}{\partial \xi}\right) + \frac{1}{\delta^2}\frac{\partial}{\partial \eta}\left(k_\eta \frac{\partial T}{\partial \eta}\right) + \frac{2k_\eta}{\delta R h_1}\frac{\partial T}{\partial \eta} = \rho c_p\left(\frac{\partial T}{\partial \tau} + \frac{\dot{m}\eta}{\delta \rho}\frac{\partial T}{\partial \eta}\right) \tag{25}$$

The boundary conditions at $\xi = 0$ are, at $\eta = 0$,

$$\frac{k_\eta}{\delta}\frac{\partial T}{\partial \eta} = \rho'' c_p'' t''\frac{\partial T}{\partial \tau} + \sigma\epsilon''\left(T^4 - T_B^4\right) \tag{26}$$

and, at $\eta = 1$,

$$\frac{k_\eta}{\delta}\frac{\partial T}{\partial \eta} = q_{net} \tag{27}$$

METHOD OF SOLUTION

The differential equations that define the temperature field in an ablating axisymmetric body of revolution are given in the previous section. To obtain a solution, these equations have been approximated by finite-difference equations and programed for solution on a high-speed digital computer. The methods used to derive the finite-difference

expressions are given in appendix C along with a summary of the finite-difference equations obtained by these methods.

The method of solution of the unknown temperature field defined by equations (C23) to (C31) is essentially that used in reference 12. This method is classed as an alternating-direction implicit method which has the advantages of being implicit, stable, and amenable to rapid solution. With this method, the second derivative $\partial^2 T/\partial y^2$ is replaced by a second difference evaluated in terms of unknown temperatures at time $\tau + \Delta\tau$, and the other derivative $\partial^2 T/\partial x^2$ is replaced by a second difference evaluated in terms of known temperatures at time τ. This formulation is implicit in the y-direction. The procedure is then repeated for a second time step of equal size, with the formulation implicit in the x-direction. The alternation in solution, that is, column-row, is continued over the specified time period. It should be noted that to maintain a stable numerical solution, a pair of successive row-column solutions is required. Successive pairs of solutions, however, may have different time steps if desired.

Equations (C23) to (C31) take the form, for either a row or a column solution, of

$$A_j T_{j-1} + B_j T_j + C_j T_{j+1} = D_j \tag{28}$$

where $j = 1, 2, 3, \ldots, S$ for the column solution and $j = 1, 2, 3, \ldots, L$ for the row solutions. Equation (28) represents L or S equations and L or S unknown temperatures. Since equation (28) results in a tridiagonal matrix of unknown temperatures, this set of equations can be quickly solved simultaneously by using a procedure based on the Gauss elimination method. This procedure is discussed in reference 12.

RESULTS AND DISCUSSION

In the following section, the accuracy of the solution for the unknown temperature field defined by equations (C23) to (C31) is evaluated by comparing the results of the numerical solution with two exact solutions. Also, the results obtained by application of the present analysis via the associated computer program to several special two-dimensional ablation cases are presented. Computer-drawn curves showing the computed results for some of these cases illustrate the plotting feature of the program.

Comparison With Exact Solutions

The exact solutions to two heat-transfer problems are used to evaluate the accuracy of the numerical results. The exact solution of an orthotropic ablating body with temperature-dependent properties is not available. Therefore, comparisons are made with results from exact solutions for homogeneous, nonablating bodies with constant properties.

Insulated thick-walled hemisphere.- The exact steady-state temperature distribution of the insulated thick-walled hemisphere shown schematically in figure 4 is derived in appendix D in spherical coordinates and is

$$T(r,\theta) = \frac{4}{3}T_o + \frac{T_o\left(3\cos^2\theta - 1\right)}{3\left[(R+\delta)^2 + \frac{2}{3}R^5(R+\delta)^{-3}\right]}\left(r^2 + \frac{2}{3}R^5 r^{-3}\right) \tag{29}$$

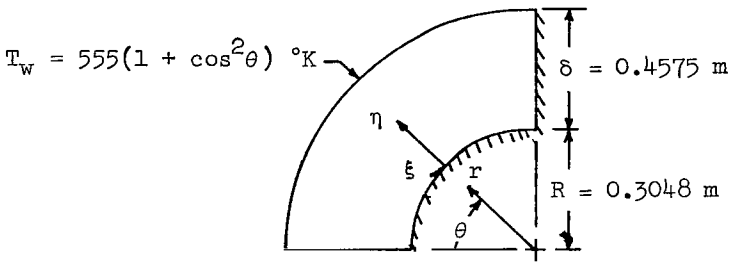

Figure 4.- Insulated thick-walled hemisphere.

The results of a comparison between the exact steady-state case and the numerical analysis with a 10- by 10-node network are shown in table 1. The fact that the error is no greater than about ±0.5 percent indicates that the errors introduced by the finite-difference pattern are small.

TABLE I.- TEMPERATURE DISTRIBUTIONS OF THICK-WALLED HEMISPHERE FROM EXACT SOLUTION AND FROM NUMERICAL ANALYSIS

η	Percent error, $\frac{T_{exact} - T_{calc}}{T_{exact}} \times 100$, for values of ξ of –								
	0	0.125	0.25	0.375	0.50	0.625	0.75	0.875	1.00
0	-0.162	-0.220	-0.234	-0.240	-0.243	-0.248	-0.257	-0.274	-0.298
.25	-.488	-.507	-.473	-.407	-.318	-.280	-.136	-.088	-.095
.50	-.467	-.493	-.463	-.397	-.304	-.194	-.093	-.034	-.048
.75	-.356	-.395	-.381	-.338	-.265	-.168	-.067	-.007	-.037
1.00	-.209	-.248	-.254	-.245	-.210	-.143	-.058	-.003	-.046

One-dimensional insulated slab.- The exact transient temperature distribution in a one-dimensional insulated slab shown schematically in figure 5(a) is given by equation (A11) in reference 13 as (in the notation of the present paper)

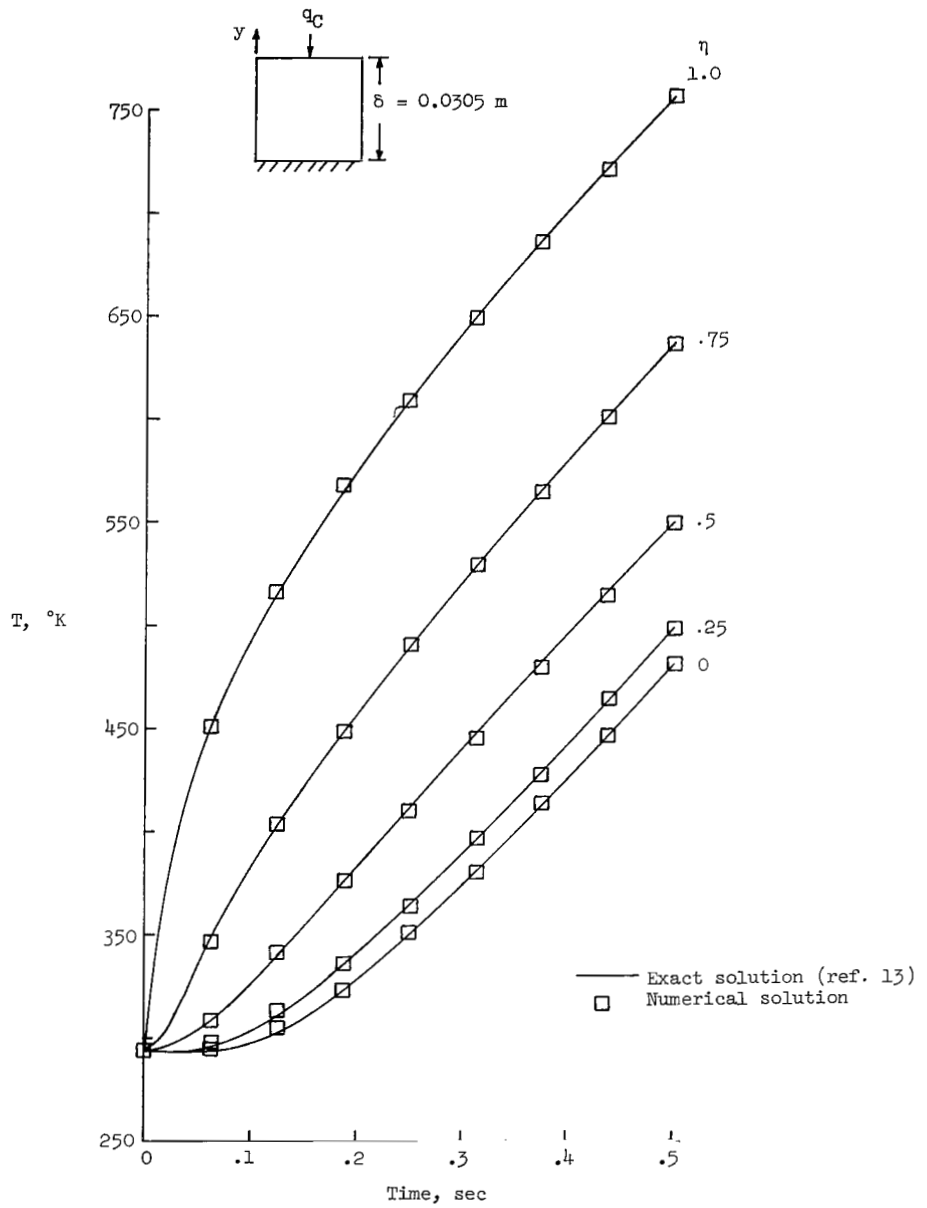

(a) Time step, 0.0625 sec.

Figure 5.- Transient temperature histories for a one-dimensional insulated slat. q_c = 1.1349 MW/m^2; k = 62.35 W/m-°K; ρ = 160.1 kg/m^3; c_p = 0.4187 J/g-°K.

$$T(y,\tau) = T_o + \frac{q_C \delta}{k_y}\left[\frac{k_y \tau}{\rho c_p \delta^2} + \frac{1}{2}\left(\frac{y}{\delta}\right)^2 - \frac{1}{6} - \frac{2}{\pi^2}\sum_{n=1}^{\infty}\frac{(-1)^n}{n^2}\cos\left(\frac{n\pi y}{\delta}\right)\exp\left(\frac{-n^2\pi^2 k\tau}{\rho c_p \delta^2}\right)\right] \qquad (30)$$

This equation gives the temperature at a point y as a function of time. Constant thermophysical properties were used for the slab (see fig. 5(a)) and the numerical values were chosen to facilitate computations and not to represent any particular material.

Comparisons between the exact solution and the numerical solution for two different time steps, 0.0625 and 0.25 second, are shown in figures 5(a) and 5(b). The numerical results are in good agreement with the exact results for both time steps.

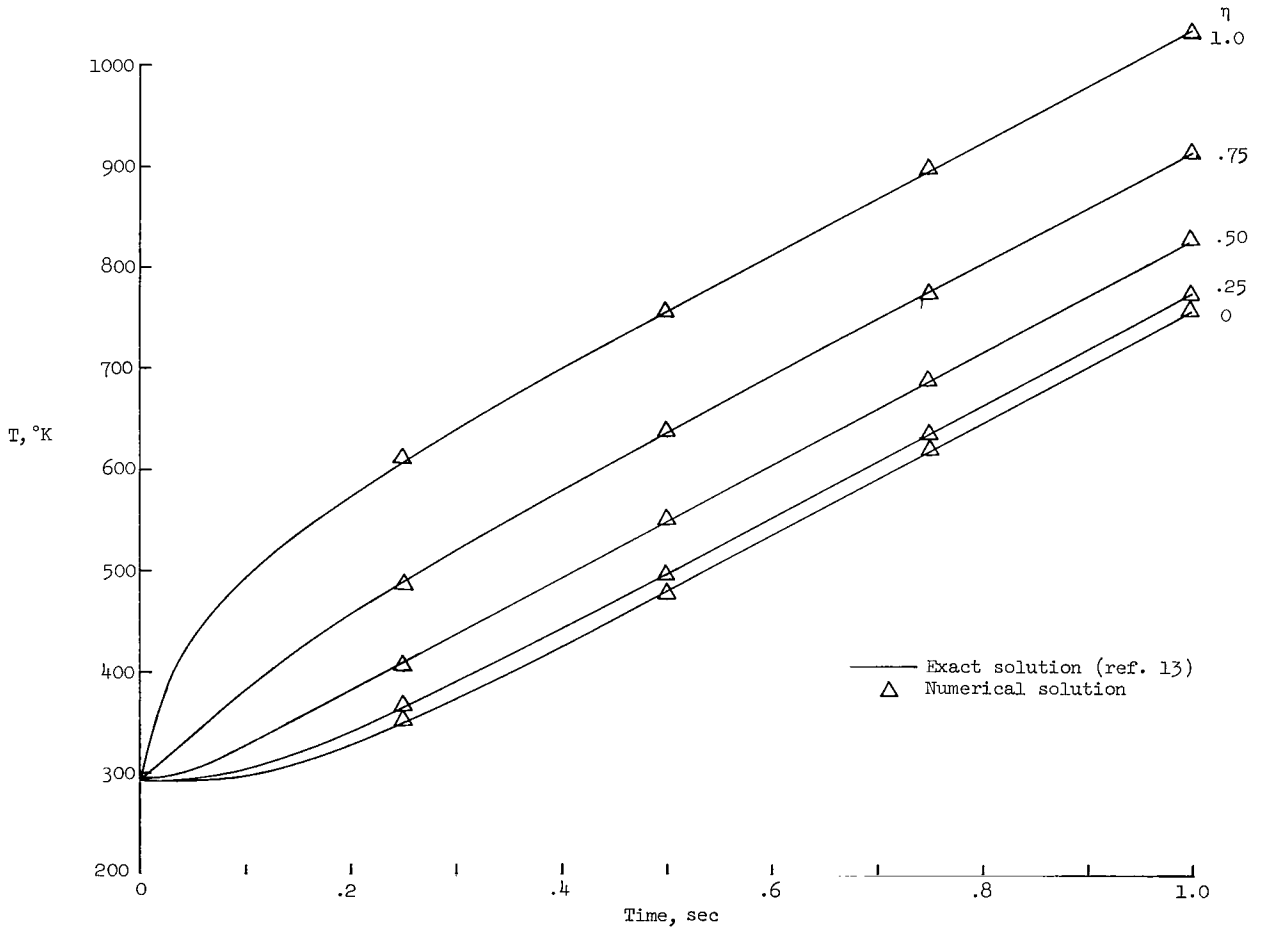

(b) Time step, 0.25 sec.

Figure 5.- Concluded.

The agreement between numerical and exact results for the larger time steps is not as good as that obtained with the smaller time step. The maximum errors for the first three time steps of 0.0625 second were, respectively, 0.70, 0.36, and 0.25 percent, whereas the maximum errors for the larger time step were -1.22, 0.56, and 0.26 percent. In both cases, the solutions were stable and converged rapidly.

Application

The results obtained from application of the present analysis to ablating bodies are presented in this section. Two of the cases discussed, an ablating hemisphere-cone body and an ablating hemisphere, are of general interest. Two additional cases provide a comparison, on a qualitative and quantitative basis, between test and analytical results. All the cases illustrate situations that are not amenable to a one-dimensional analysis.

Hemisphere-cone body.- A graphite hemisphere-cone body is exposed to stagnation convective and radiant heating rates of 34 and 11 MW/m^2, respectively, and a stream enthalpy of 93 MJ/kg. These energy levels are typical of earth entry at hyperbolic velocities. The body is assumed to be subjected to this environment for 60 seconds. Figure 6(a) shows computed geometry as a function of time during the 60-second exposure.

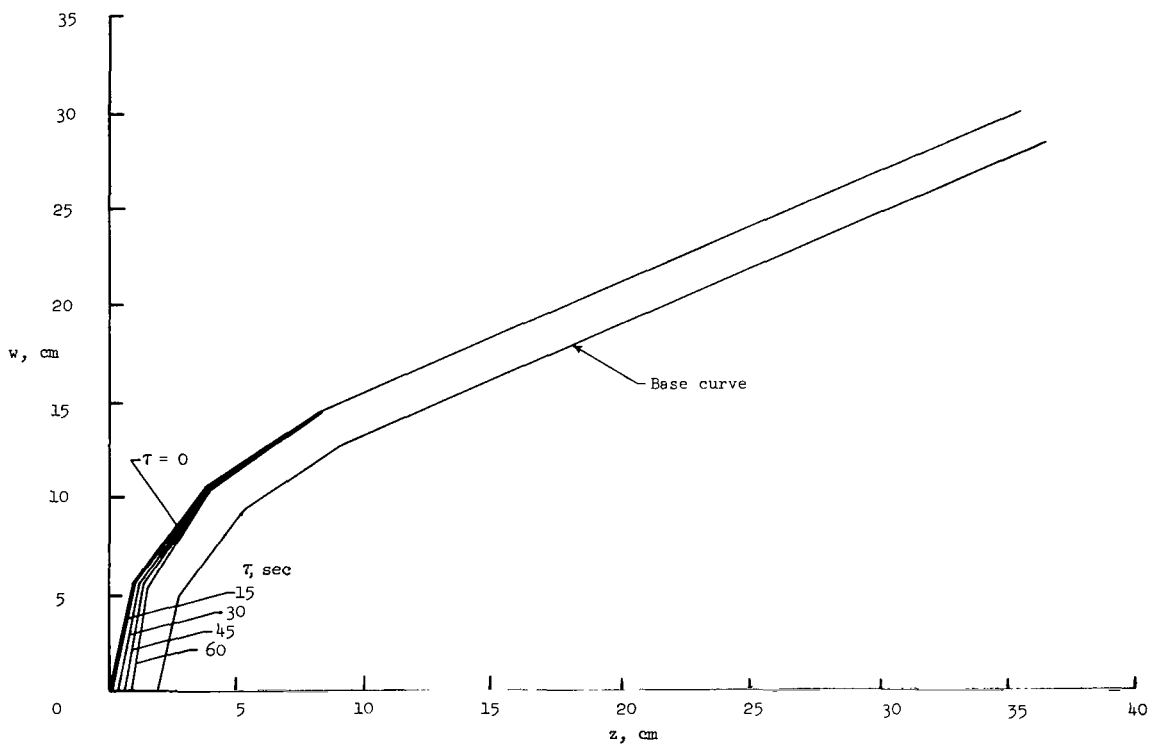

(a) Shape change.

Figure 6.- Graphite hemisphere-cone body. Initial stagnation cold-wall heating rates of q_c = 34 MW/m^2 and q_r = 11 MW/m^2; H_e = 93 MJ/kg; in air.

Note the nonuniform surface recession over the body which requires continued adjustment in pressure and heating-rate distributions over the body. Adjustments to the stagnation heating rates are required to account for increased nose bluntness. These latter adjustments, as computed with the present analysis, are shown in figure 6(b).

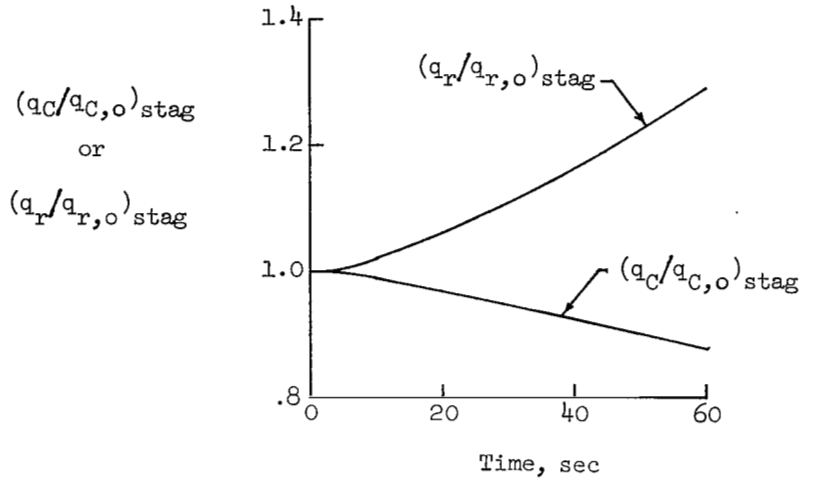

(b) Variation of stagnation heating rates (due to changing nose bluntness) with time.

Figure 6.- Concluded.

A 5- by 10-node network, that is, $S = 5$ and $L = 10$, was used for this example. A finer network would produce smoother profiles of the hemisphere-cone body than are shown in figure 6(a). This is particularly true in the hemispherical portion of the body. The total number of stations that should be used will depend on the physical size of the body considered and the gradients of the surface inputs, that is, heating rates and pressure on the surface.

Hemisphere.- A low-density phenolic-nylon hemisphere, approximated with a 10- by 10-node network, is assumed to be exposed to a convective heating rate of 3.4 MW/m^2 in air for 110 seconds. The method presented in reference 7 was used to approximate the thermophysical and thermochemical properties of a charring ablator in a single-layer material.

Figure 7(a) shows the outer surface location as a function of time. For these calculations the heating-rate distribution was based on Newtonian pressure distribution, and therefore, figure 7(a) shows qualitative rather than quantitative results for an ablating hemisphere. Note that for about the first 70 seconds, nonuniform ablation occurs across the surface; however, after 70 seconds, the recession is uniform. This behavior, although expected, would not be revealed in a one-dimensional analysis or a multidimensional analysis that does not consider shape change. Similarly, the variation in the stagnation heating rate with nose bluntness would not be revealed in a one-dimensional analysis or a

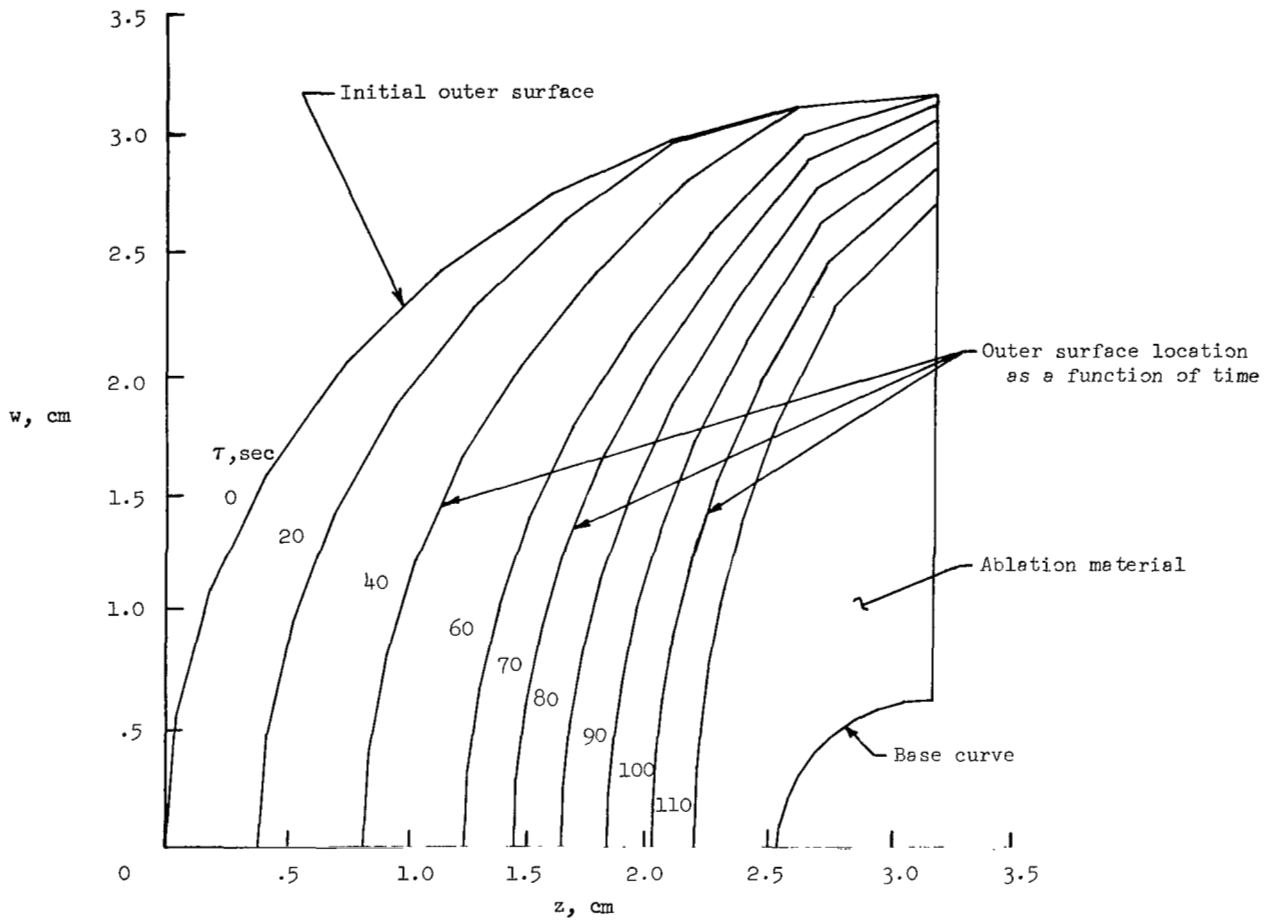

(a) Shape change.

Figure 7.- Hemispherical nose cap of low-density phenolic-nylon. Initial stagnation cold-wall convective heating rate of 3.4 MW/m^2; H_e = 7 MJ/kg; in air.

multidimensional analysis that does not consider shape change. The variation in the stagnation heating rate with time resulting from nose bluntness, as computed by the present analysis, is shown in figure 7(b).

Teflon sphere.- The results of a series of tests on teflon spheres at various heating conditions are given in reference 14. One of the spheres, model E, was tested at an initial stagnation cold-wall convective heating rate of 6.41 MW/m^2, a stream enthalpy of 4.88 MJ/kg, and a Mach number of 2.6. The experimental profile history for model E is shown in figure 8(a).

The analytical profile history for model E, obtained by using the present analysis with a 10- by 10-node network, is shown in figure 8(b). The agreement between the

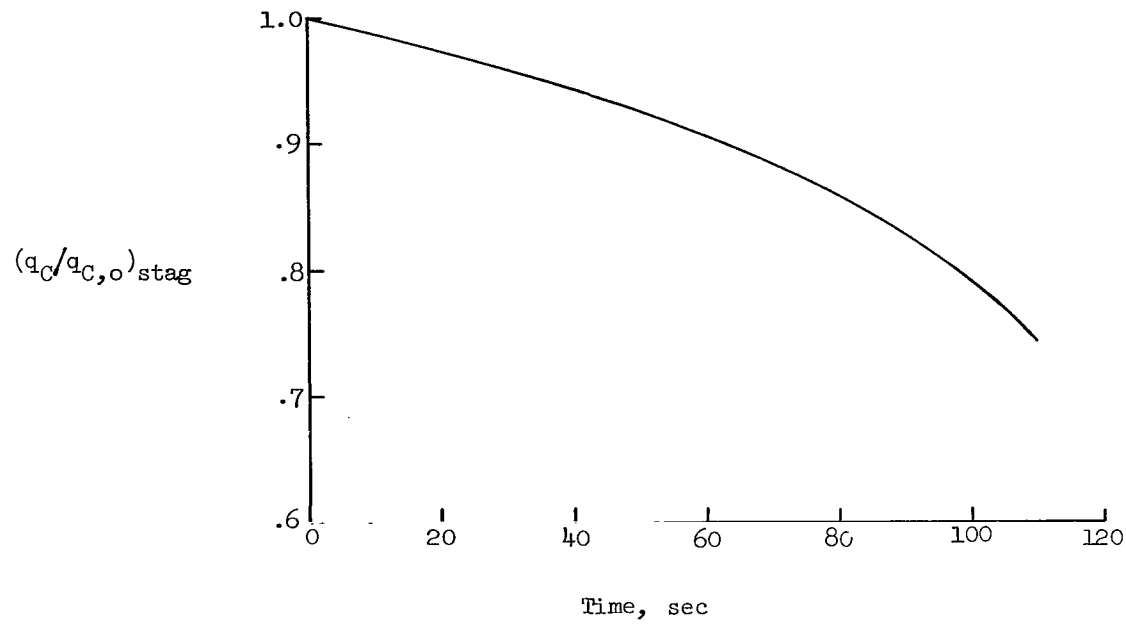

(b) Variation of stagnation heating rate (due to changing nose bluntness) with time.

Figure 7.- Concluded.

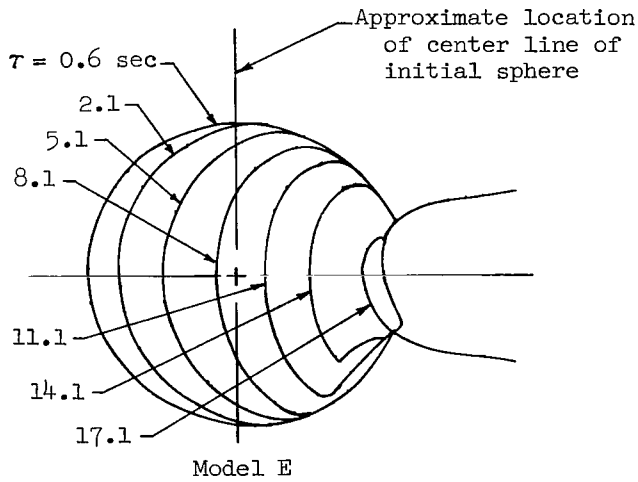

(a) Experimental profile history (ref. 14).

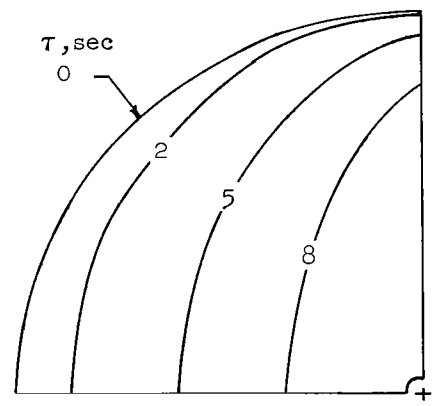

(b) Analytical profile history.

Figure 8.- Experimental and analytical profile histories for an ablating teflon sphere. Initial conditions: $q_{c,stag}$ = 6.41 MW/m^2; H_e = 4.88 MJ/kg; Mach number, 2.6.

experimental and analytical profile histories is good, qualitatively, up to about 8 seconds. The analytical calculations were terminated at 8 seconds because the present analysis cannot consider the entire sphere, but only the forward hemisphere. Therefore, in the analysis the stagnation point cannot recede more than a length equal to one body radius. Also, the heating-rate distribution used is not accurate for highly blunted bodies.

A comparison between the experimental and analytical stagnation-point recession is shown in figure 9. The analytical and experimental recessions are in good agreement. This agreement is better quantitatively than that shown in figure 8 because the inaccurate heating-rate distribution predicted with the present method for highly blunted bodies did not affect stagnation-point recession as directly as it affected the overall recession.

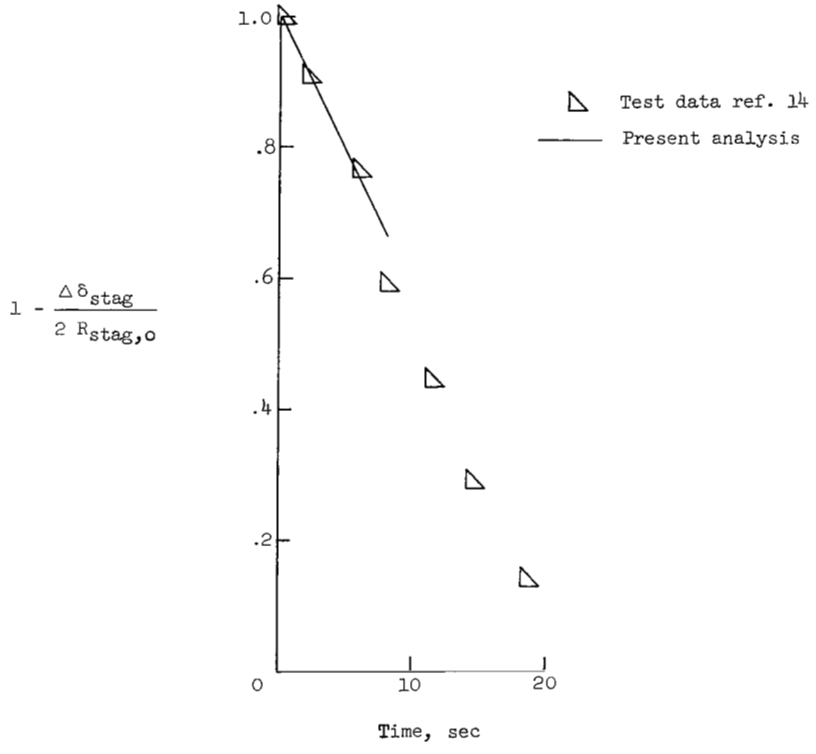

Figure 9.- Comparison between the experimental and analytical stagnation-point recession for an ablating teflon sphere. Initial conditions: $q_{C,stag} = 6.41$ MW/m^2; $H_e = 4.88$ MJ/kg; Mach number, 2.6.

Laser test.- The results of tests of a low-density phenolic-nylon ablation material at high radiant heating rates produced by a laser beam are given in reference 15. The specimen was exposed to a laser beam, with the energy distribution shown in figure 10(a), for 2 seconds. The maximum radiant heating rate at the center was about 40 MW/m^2. The final geometry of the ablated specimen was characterized by a very thin shell of charred material, figure 10(b). The present analysis was used to determine whether

sufficient radiation from the sides could limit recession along the sides and thus allow a thin shell of char to remain.

The profiles computed first by assuming no radiation from the specimen sides and then by assuming that the sides radiate are shown in figure 10(c). Note that without radiation, the cusp profile is similar to that obtained during the test except that the sides are not as high. When the sides are allowed to radiate, the center recedes about the same

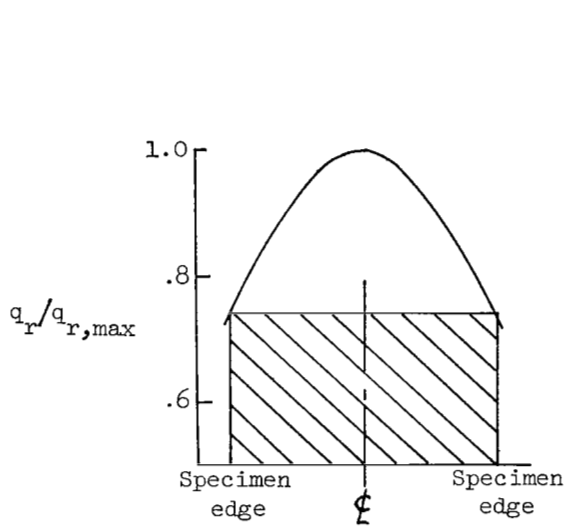

(a) Energy distribution.

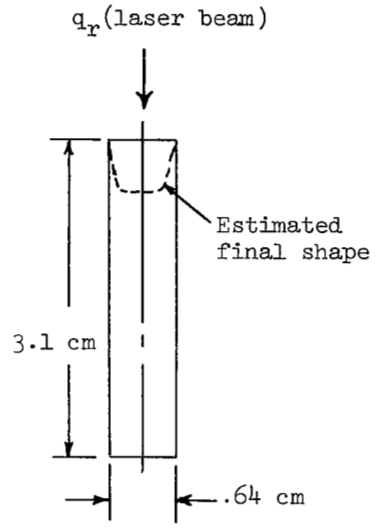

(b) Estimated specimen shape.

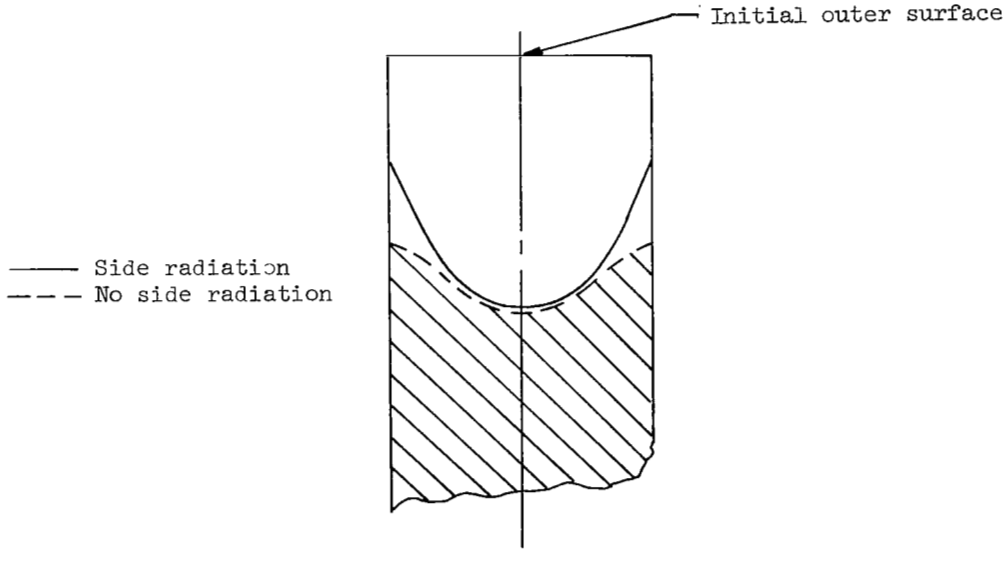

(c) Calculated recession.

Figure 10.- Laser test results for low-density phenolic-nylon specimen (ref. 15).

amount as with no radiation; however, tall sides, more characteristic of the experimental results, are obtained. This substantiates the conclusion drawn in reference 15 that the sides of the model were cooled sufficiently by radiation to permit a considerable height of char to remain at the edges.

The profiles shown in figure 10(c) were computed with a 10- by 5-node network (i.e., $S = 10$ and $L = 5$). The computation was repeated with a 10- by 10-node network with essentially the same results.

CONCLUDING REMARKS

The differential equations governing the transient response of an ablating axisymmetric, orthotropic body have been derived for fixed points in a moving coordinate system. These equations have been expanded into finite-difference form and have been programed for numerical solution with an implicit technique on a digital computer. Numerical results compared favorably with the exact solutions for simplified conduction problems.

The determination of the changes in the body geometry as ablation occurs, and the effect of these changes on the surface energy inputs, is a salient feature of this analysis. This feature was used to obtain satisfactory agreement between numerical and experimental results of an ablating teflon sphere and a small test specimen exposed to a high-intensity laser beam.

Langley Research Center,
National Aeronautics and Space Administration,
Hampton, Va., April 2, 1971.

APPENDIX A

SHAPE CHANGE DUE TO MASS LOSS

Mass transfer at the surface due to ablation causes a change in material thickness. The change in material thickness at any point n on the surface is, from equation (18),

$$\delta_n = \delta_{n,o} - \int_0^\tau \frac{\dot{m}_n}{\rho} d\tau \tag{A1}$$

When there are variations in heating and pressure over the body surface, the mass transfer also varies over the surface. This variation in mass transfer causes a nonuniform change in thickness and, hence, a change in shape which consequently alters the heating-rate and pressure distributions over the surface.

The heating-rate and pressure distributions are recalculated, with the analysis of reference 11, as the shape changes. The methods used to evaluate the shape parameters w_n, ψ_n, and R_{stag} required to implement the analysis of reference 11 are given in this appendix.

The w,z coordinate system shown in figure 2 is used to define the surface geometry at any time. The surface coordinates at station n as a function of time are

$$w(\tau) = R_{cyl} + \delta(\tau)\cos\theta \tag{A2}$$

and

$$z(\tau) = z(\tau)_o + \delta(\tau)_o - \delta(\tau)\sin\theta \tag{A3}$$

The instantaneous value of the angle ψ_n between the free-stream velocity vector and the local normal to the surface is required in defining a new pressure distribution. This angle is determined as follows:

For $n = 1$,

$$\psi_1 = 0 \tag{A4}$$

for $2 \leq n < L$,

$$\psi_n = 90^o - \tan^{-1}\left(\frac{w_{n+1} - w_{n-1}}{z_{n+1} - z_{n-1}}\right) \tag{A5}$$

and for $n = L$,

$$\psi_L = 90^o - \tan^{-1}\left(\frac{w_L - w_{L-1}}{z_L - z_{L-1}}\right) \tag{A6}$$

Both the stagnation convective and radiative heating rates are functions of the instantaneous radius of curvature. The radius of curvature in the stagnation region is obtained by finding the radius of a circle passing through points (S,1) and (S,2) (see fig. 11) in w,z coordinates.

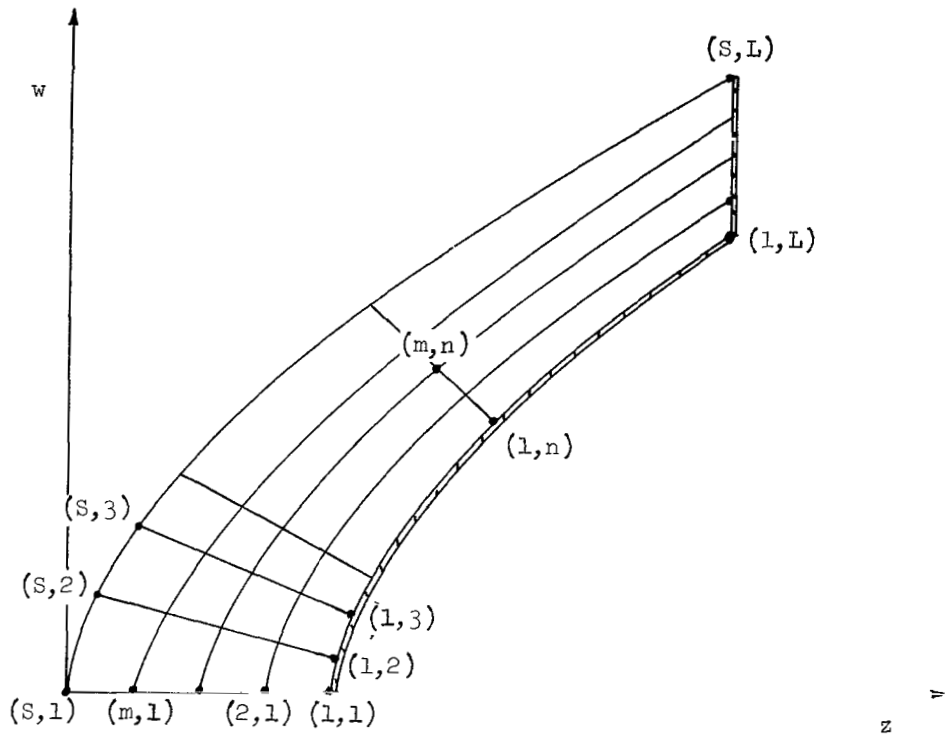

Figure 11.- Location of finite-difference stations.

The equation of a circle in the w,z coordinate system with its center on the z-axis is of the form

$$\left[z - \left(z_1 + R_{stag}\right)\right]^2 + w^2 = R_{stag}^2 \tag{A7}$$

Evaluating equation (A7) at the point (S,2) and solving for R_{stag} gives the radius of curvature in the stagnation region as

$$R_{stag} = \frac{z_2^2 - 2z_2z_1 + z_1^2 + w_2^2}{2\left(z_2 - z_1\right)} \tag{A8}$$

APPENDIX B

DERIVATION OF THE DIFFERENTIAL EQUATIONS AT THE COORDINATE SINGULARITY

The governing differential equation, equation (3), has a line of singularity at $x = 0$. This singularity can be eliminated by examining the behavior of the scale factor h_3 as $x \to 0$.

As $x \to 0$, $R_{cyl} \to x$ and $\cos\theta = \frac{R_{cyl}}{R} \to \frac{x}{R}$. Therefore,

$$h_3 = R_{cyl} + y\cos\theta \to x\left(1 + \frac{y}{R}\right) = xh_1 \tag{B1}$$

$$\left(\frac{\partial h_3}{\partial x}\right)_{x\to 0} = h_1 \tag{B2}$$

and

$$\left(\frac{\partial h_3}{\partial y}\right)_{x\to 0} = \frac{x}{R} \tag{B3}$$

Now consider equation (3) in the expanded form

$$\frac{1}{h_1}\frac{\partial}{\partial x}\left(\frac{k_x}{h_1}\frac{\partial T}{\partial x}\right) + \frac{k_x}{h_1^2 h_3}\frac{\partial T}{\partial x}\frac{\partial h_3}{\partial x} + \frac{1}{h_1}\frac{\partial}{\partial y}\left(h_1 k_y \frac{\partial T}{\partial y}\right) + \frac{k_y}{h_3}\frac{\partial T}{\partial y}\frac{\partial h_3}{\partial y} = \rho c_p \frac{\partial T}{\partial \tau} \tag{B4}$$

As $x \to 0$, equations (B1), (B2), and (B3) reduce equation (B4) to

$$\frac{1}{h_1}\frac{\partial}{\partial x}\left(\frac{k_x}{h_1}\frac{\partial T}{\partial x}\right) + \frac{k_x}{h_{1x}^2}\frac{\partial T}{\partial x} + \frac{1}{h_1}\frac{\partial}{\partial y}\left(h_1 k_y \frac{\partial T}{\partial y}\right) + \frac{k_y}{Rh_1}\frac{\partial T}{\partial y} = \rho c_p \frac{\partial T}{\partial \tau} \tag{B5}$$

At $x = 0$, the axisymmetric-body assumption requires that $\frac{\partial T}{\partial x} = 0$ and $\frac{\partial h_1}{\partial x} = 0$. As a result, the second term on the left side of equation (B5) becomes indeterminate. Applying L'Hospital's rule to this term gives

$$\lim_{x\to 0} \frac{k_x \frac{\partial T}{\partial x}}{h_{1x}^2} = \frac{k_x}{h_1^2}\frac{\partial^2 T}{\partial x^2} \tag{B6}$$

Equation (B5) may now be written as

$$\frac{2k_x}{h_1^2}\frac{\partial^2 T}{\partial x^2} + \frac{\partial}{\partial y}\left(k_y \frac{\partial T}{\partial y}\right) + \frac{2k_y}{Rh_1}\frac{\partial T}{\partial y} = \rho c_p \frac{\partial T}{\partial \tau} \tag{B7}$$

which is the governing differential equation along the line $x = 0$ and is solved with the boundary conditions of equations (19) and (22).

APPENDIX C

FINITE-DIFFERENCE EQUATIONS

The differential equations are put in finite-difference form through the use of Taylor's series expansions. Forward, central, and backward differences are used. The methods used to obtain these differences are from reference 8. These methods, in general, use Taylor's series expansions at points $\pm\Delta\xi$ or $\pm\Delta\eta$ to evaluate first-order derivatives and Taylor's series expansions at points $\pm\Delta\xi/2$ or $\pm\Delta\eta/2$ to evaluate second-order derivatives. Typical finite-difference expressions used are summarized in this appendix. The sketches in figure 12 illustrate the spatial relationship between points used in the Taylor's series expansions.

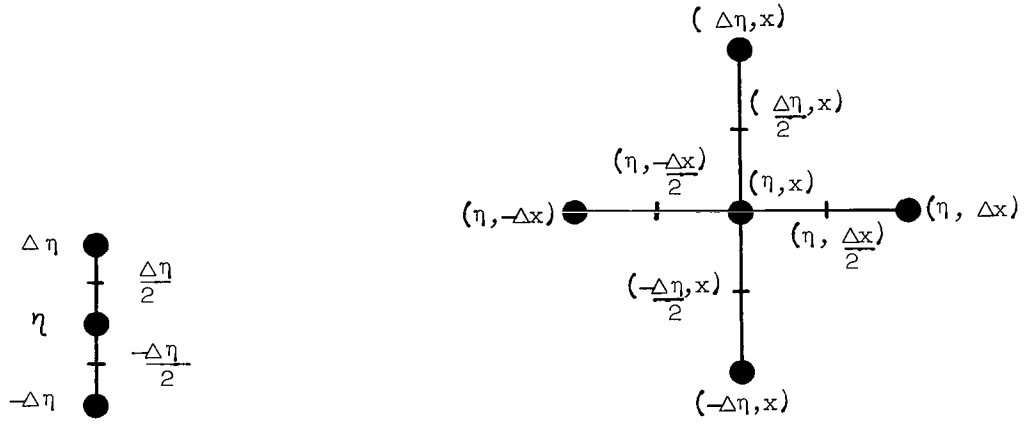

(a) For standard derivatives. (b) For cross derivatives.

Figure 12.- Spatial relation between points used in Taylor's series expansions.

First-Order Derivatives

The first-order derivatives are given by the following equations which are correct to order of $\Delta\eta^2$:

Forward difference

$$\left.\frac{\partial T}{\partial \eta}\right|_{\eta} = \frac{4T_{\Delta\eta} - 3T_{\eta} - T_{2\Delta\eta}}{2\,\Delta\eta} \tag{C1}$$

Central difference

$$\left.\frac{\partial T}{\partial \eta}\right|_{\eta} = \frac{T_{\Delta\eta} - T_{-\Delta\eta}}{2\,\Delta\eta} \tag{C2}$$

Backward difference

$$\left.\frac{\partial T}{\partial \eta}\right|_{\eta} = \frac{3T_{\eta} - 4T_{-\Delta\eta} + T_{-2\Delta\eta}}{2\,\Delta\eta} \tag{C3}$$

Second-Order Derivatives

The second-order derivatives are given by the following equations:

Forward difference

$$\frac{\partial}{\partial \eta}\left(B\,\frac{\partial T}{\partial \eta}\right)_{\eta} = \frac{9B_{\Delta n/2}\left(T_{\Delta\eta} - T_{\eta}\right) - B_{3\Delta\eta/2}\left(T_{2\Delta\eta} - T_{\Delta\eta}\right) - 8\,\Delta\eta\left(B\,\frac{\partial T}{\partial \eta}\right)_{\eta}}{3\,\Delta\eta^2} \tag{C4}$$

where $B = h_1 h_3 k$.

Central difference

$$\frac{\partial}{\partial \eta}\left(B\,\frac{\partial T}{\partial \eta}\right)_{\eta} = \frac{B_{\Delta\eta/2}\left(T_{\Delta\eta} - T_{\eta}\right) - B_{-\Delta\eta/2}\left(T_{\eta} - T_{-\Delta\eta}\right)}{\Delta\eta^2} \tag{C5}$$

Backward difference

$$\frac{\partial}{\partial \eta}\left(B\,\frac{\partial T}{\partial \eta}\right)_{\eta} = -\frac{9B_{-\Delta\eta/2}\left(T_{\eta} - T_{-\Delta\eta}\right) + B_{-3\Delta\eta/2}\left(T_{-\Delta\eta} - T_{-2\Delta\eta}\right) + 8\,\Delta\eta\left(B\,\frac{\partial T}{\partial \eta}\right)_{\eta}}{\Delta\eta^2} \tag{C6}$$

Cross Derivatives

The methods used to evaluate cross derivatives can be shown by considering the term

$$\frac{\partial}{\partial \eta}\left(B\,\frac{\partial T}{\partial x}\right) \tag{C7}$$

Term (C7) is first expanded in the η-direction. Thus,

$$\frac{\partial}{\partial \eta}\left(B\,\frac{\partial T}{\partial x}\right)_{\eta,x} = \frac{B\,\left.\frac{\partial T}{\partial x}\right|_{\Delta\eta,x} - B\,\left.\frac{\partial T}{\partial x}\right|_{-\Delta\eta,x}}{2\,\Delta\eta} \tag{C8}$$

The first derivatives are then expanded in the x-direction to give

$$\frac{\partial}{\partial\eta}\left(B\frac{\partial T}{\partial x}\right)_{\eta,x} = \frac{B_{\Delta\eta,x}\left(T_{\Delta\eta,\Delta x} - T_{\Delta\eta,-\Delta x}\right) - B_{-\Delta\eta,x}\left(T_{-\Delta\eta,\Delta x} - T_{-\Delta\eta,-\Delta x}\right)}{4\,\Delta\eta\,\Delta x} \tag{C9}$$

Equation (C9) is correct to $\Delta\eta^2$, Δx^2. Equations (C8) and (C9) are central-difference expansions.

The forward expansion of term (C7) is obtained by evaluating at $\Delta\eta$ and $2\,\Delta\eta$, which gives

$$\frac{\partial}{\partial\eta}\left(B\frac{\partial T}{\partial x}\right)_{\eta,x} = \frac{4B\left.\frac{\partial T}{\partial x}\right|_{\Delta\eta,x} - 3B\left.\frac{\partial T}{\partial x}\right|_{\eta,x} - B\left.\frac{\partial T}{\partial x}\right|_{2\Delta n,x}}{2\,\Delta\eta} \tag{C10}$$

The first derivatives are then expanded to give

$$\frac{\partial}{\partial\eta}\left(B\frac{\partial T}{\partial x}\right)_{\eta,x} = \frac{4B_{\Delta\eta,x}\left(T_{\Delta\eta,\Delta x} - T_{\Delta\eta,-\Delta x}\right) - 3B_{\eta,x}\left(T_{\eta,\Delta x} - T_{\eta,-\Delta x}\right) - B_{2\Delta\eta,x}\left(T_{2\Delta\eta,\Delta x} - T_{2\Delta\eta,-\Delta x}\right)}{4\,\Delta\eta\,\Delta x} \tag{C11}$$

The backward expansion of term (C7) is obtained by evaluating at $-\Delta\eta$ and $-2\,\Delta\eta$. The resulting expression is

$$\frac{\partial}{\partial\eta}\left(B\frac{\partial T}{\partial x}\right)_{\eta,x} = \frac{3B_{\eta,x}\left(T_{\eta,\Delta x} - T_{\eta,-\Delta x}\right) - 4B_{-\Delta\eta,x}\left(T_{-\Delta\eta,\Delta x} - T_{-\Delta\eta,-\Delta x}\right) + B_{-2\Delta\eta,x}\left(T_{-2\Delta\eta,\Delta x} - T_{-2\Delta\eta,-\Delta x}\right)}{4\,\Delta\eta\,\Delta x} \tag{C12}$$

A Special Case

The boundaries along $x = 0$ and $x = L$ require special attention. At these two locations the boundary conditions are, respectively,

$$\frac{k_x}{h_1}\frac{DT}{\partial x} = \left(\frac{1}{x_b}\frac{\partial T}{\partial\xi} - \frac{\eta A}{\delta}\frac{\partial T}{\partial\eta}\right) = 0 \tag{C13}$$

and

$$\frac{k_x}{h_1}\frac{DT}{\partial x} = -\rho' c_p' t'\frac{\partial T}{\partial\tau} - \sigma\epsilon'\left(T_{m,L}^4 - T_B^4\right) \tag{C14}$$

Because of symmetry at $x = 0$,

$$A = \frac{\partial \delta}{\partial x} = 0 \tag{C15}$$

Therefore, at $x = 0$, the boundary condition becomes

$$\frac{DT}{\partial x} = \frac{1}{x_b} \frac{\partial T}{\partial \xi} = 0 \tag{C16}$$

A forward-difference expansion different from equation (C8) can now be obtained for the first term on the left side of equation (25). This difference expression of $\partial^2 T/\partial x^2$ is obtained as follows: A Taylor's series expansion of $T_{m,2}$ in terms of $T_{m,1}$ is

$$T_{m,2} = T_{m,1} + \Delta x \frac{\partial T_{m,1}}{\partial x} + \frac{\Delta x^2}{2} \frac{\partial^2 T_{m,1}}{\partial x^2} + \frac{\Delta x^3}{6} \frac{\partial^3 T_{m,1}}{\partial x^3} + \frac{\Delta x^4}{24} \frac{\partial^4 T_{m,1}}{\partial x^4} + \cdots \tag{C17}$$

Similarly, the expansion of $T_{m,3}$ in terms of $T_{m,1}$ is

$$T_{m,3} = T_{m,1} + 2\,\Delta x \frac{\partial T_{m,1}}{\partial x} + \frac{4\,\Delta x^2}{2} \frac{\partial^2 T_{m,1}}{\partial x^2} + \frac{8\,\Delta x^3}{6} \frac{\partial^3 T_{m,1}}{\partial x^3} + \frac{16}{24} \Delta x^4 \frac{\partial^4 T_{m,1}}{\partial x^4} + \cdots \tag{C18}$$

Eliminating the third derivative between equations (C17) and (C18) gives

$$8T_{m,2} - T_{m,3} = 7T_{m,1} + 6\,\Delta x \frac{\partial T_{m,1}}{\partial x} + \frac{4\,\Delta x^2}{2} \frac{\partial^2 T_{m,1}}{\partial x^2} - \frac{8}{24} \Delta x^4 \frac{\partial^4 T_{m,1}}{\partial x^4} + \cdots \tag{C19}$$

After the boundary condition of equation (C16) is utilized, equation (C19) becomes

$$\frac{\partial^2 T_{m,1}}{\partial x^2} = \frac{8T_{m,2} - T_{m,3} - 7T_{m,1}}{2\,\Delta x^2} \tag{C20}$$

Along $x = L$, it is advantageous to write the first term in equation (3) in a semi-expanded form, which is, in the ξ,η coordinates,

$$\frac{D}{\partial x}\left(B \frac{DT}{\partial x}\right) = \left(\frac{1}{x_b} \frac{\partial}{\partial \xi} - \eta \frac{A}{\delta} \frac{\partial}{\partial \eta}\right)\left(B \frac{DT}{\partial x}\right) = \frac{1}{x_b} \frac{\partial}{\partial \xi}\left(B \frac{DT}{\partial x}\right) - \eta \frac{A}{\delta} \frac{\partial}{\partial \eta}\left(B \frac{DT}{\partial x}\right) \tag{C21}$$

when a half-station backward-difference expression (eq. (C10)) is used, the first term on the right side of equation (C21) becomes

$$\frac{-3B_{-\Delta x/2}\left(\frac{DT}{\partial x}\right)_{-\Delta x/2}}{x_b\,\Delta\xi} + \frac{B_{-3\Delta x/2}\left(\frac{DT}{\partial x}\right)_{-3\Delta x/2}}{x_b\,\Delta\xi} + \frac{8}{3x_b\,\Delta\xi}\left(\frac{DT}{\partial x}\right)_x \tag{C22}$$

The last term is evaluated from the boundary condition at $x = L$ (eq. (C14)). The other terms are expressed in forward-, backward-, or central-difference form as required.

Finite-Difference Approximations of the Field Equations

The locations of the finite-difference stations (m,n) are shown in figure 11. The m and n subscripts correspond to the η-coordinates and ξ-coordinates, respectively.

The methods used to change the differential equations to finite-difference form are given in the preceding sections of this appendix. A summary of the finite-difference equations obtained by these methods is presented here.

For any point (m,n), where $1 < m < S$, $1 < n < L$, the governing equation (eq. (9)) is

$$\frac{1}{x_b^2\Delta\xi^2}\left[\left(\frac{h_3k_\xi}{h_1}\right)_{m,n+\frac{1}{2}}\left(T_{m,n+1} - T_{m,n}\right) - \left(\frac{h_3k_\xi}{h_1}\right)_{m,n-\frac{1}{2}}\left(T_{m,n} - T_{m,n-1}\right)\right]$$

$$+ \frac{1}{\delta_n^2\Delta\eta^2}\left[\left(h_1h_3k_\eta\right)_{m+\frac{1}{2},n}\left(T_{m+1,n} - T_{m,n}\right) - \left(h_1h_3k_\eta\right)_{m-\frac{1}{2},n}\left(T_{m,n} - T_{m-1,n}\right)\right]$$

$$- \frac{1}{4x_b\,\Delta\xi\,\Delta\eta}\left[\left(\frac{h_3k_\xi\eta A}{h_1\delta}\right)_{m,n+\frac{1}{2}}\left(T_{m+1,n+1} - T_{m-1,n+1} + T_{m+1,n} - T_{m-1,n}\right)\right.$$

$$\left. - \left(\frac{h_3k_\xi\eta A}{h_1\delta}\right)_{m,n-\frac{1}{2}}\left(T_{m+1,n} - T_{m-1,n} + T_{m+1,n-1} - T_{m-1,n-1}\right)\right]$$

$$- \left(\frac{\eta A k_\xi}{4\delta\,\Delta\eta x_b\,\Delta\xi}\right)_{m,n}\left[\left(\frac{h_3}{h_1}\right)_{m+1,n}\left(T_{m+1,n+1} - T_{m+1,n-1}\right) - \left(\frac{h_3}{h_1}\right)_{m-1,n}\left(T_{m-1,n+1} - T_{m-1,n-1}\right)\right]$$

(Equation continued on next page)

$$+\left(\frac{\eta A}{\delta\,\Delta\eta^2}\right)\left[\left(\frac{h_3 k_\xi \eta A}{h_1 \delta}\right)_{m+\frac{1}{2},n}\left(T_{m+1,n}-T_{m,n}\right)-\left(\frac{h_3 k_\xi \eta A}{h_1 \delta}\right)_{m-\frac{1}{2},n}\left(T_{m,n}-T_{m-1,n}\right)\right]$$

$$=\left(h_1 h_3 \rho c_p\right)_{m,n}\left[\frac{\Delta T_{m,n}}{\Delta\tau}+\left(\frac{\eta\dot{m}}{\delta\rho}\right)_{m,n}\frac{\left(T_{m+1,n}-T_{m-1,n}\right)}{2\,\Delta\eta}\right] \tag{C23}$$

At station (m = 1, n = 1), the boundary condition (eq. (26)) is combined with equation (25) to give

$$\left(\frac{k_\xi}{h_1^2}\right)_{1,1}\frac{a}{x_b^2}\left(\frac{8T_{1,2}-T_{1,3}-7T_{1,1}}{2\,\Delta\xi^2}\right)+\frac{1}{\delta_{1,1}^2}\left\{\frac{9(k\eta)_{3/2,1}\left(T_{2,1}-T_{1,1}\right)}{3\,\Delta\eta^2}\right.$$

$$\left.-\frac{(k\eta)_{5/3,1}\left(T_{3,1}-T_{2,1}\right)}{3\,\Delta\eta^2}-\frac{8}{3\,\Delta\eta}\delta_{1,1}\left[\rho'' c_p'' t''\frac{\Delta T_{1,1}}{\Delta\tau}+\sigma\epsilon''\left(T_{1,1}^4-T_B^4\right)\right]\right\}$$

$$=\left(\rho c_p-\frac{2}{Rh_1}\rho'' c_p'' t''\right)\left(\frac{\Delta T_{1,1}}{\Delta\tau}\right)-\frac{2\sigma\epsilon''}{Rh_1}\left(T_{1,1}^4-T_B^4\right) \tag{C24}$$

For the curvilinear coordinate system, the a term is set equal to 2. It should be noted that for Cartesian coordinates, a slight modification must be made to equations (C24), (C25), and (C26). This modification is required since there is no line of singularity in the Cartesian system as there is in the curvilinear system. The correct forms of equations (C24), (C25), and (C26) for the Cartesian system are obtained by setting the a term in these equations equal to 1.

For station (1 < m < S, n = 1), equations (24) and (25) yield

$$\left(\frac{a k_\xi}{h_1^2 x_b^2 \Delta\xi^2}\right)_{m,1}\left[\left(\frac{8T_{m,2}-T_{m,3}-7T_{m,1}}{2}\right)\right.$$

$$\left.-\left(\frac{\eta}{\delta\,\Delta\eta}\right)_{m,1}\left(\frac{T_{m+1,1}-T_{m-1,1}}{2}\right)\left(\frac{8\delta_{m,2}-\delta_{m,3}-7\delta_{m,1}}{2}\right)\right]+\left(\frac{k_\eta}{h_1 R\delta\,\Delta\eta}\right)_{m,1}\left(T_{m+1,1}-T_{m-1,1}\right)$$

$$+\left(\frac{1}{\delta^2\Delta\eta^2}\right)_{m,1}\left[(k_\eta)_{m+\frac{1}{2},1}\left(T_{m+1,1}-T_{m,1}\right)-(k_\eta)_{m-\frac{1}{2},1}\left(T_{m,1}-T_{m-1,1}\right)\right]$$

(Equation continued on next page)

$$= \left(\rho c_p\right)_{m,1} \frac{\Delta T_{m,1}}{\Delta \tau} + \left(\frac{\eta \dot{m} c_p}{2\delta\, \Delta\eta}\right)_{m,1} \left(T_{m+1,1} - T_{m-1,1}\right) \tag{C25}$$

For station (m = S, n = 1), equations (25) and (27) result in

$$\left(\frac{a k_\xi}{2x_b^2 \Delta\xi^2 h_1^2}\right)_{S,1} \left[\left(8T_{S,2} - T_{S,3} - 7T_{S,1}\right) - \left(\frac{h_2}{k_\eta}\right)_{S,1} \left(q_{net}\right)_{S,1} \left(8\delta_{S,2} - \delta_{S,3} - 7\delta_{S,1}\right)\right]$$

$$+ \left(\frac{2}{h_1 R}\right)_{S,1} \left(q_{net}\right)_{S,1} + \frac{1}{\left(3\delta^2 \Delta\eta^2\right)_{S,1}} \left[\left(k_\eta\right)_{S-\frac{3}{2},1} \left(T_{S-1,1} - T_{S-2,1}\right) - 9\left(k_\eta\right)_{S-\frac{1}{2},1} \left(T_{S,1} - T_{S-1,1}\right)\right.$$

$$\left. + 8\delta_{S,1}\, \Delta\eta \left(q_{net}\right)_{S,1}\right] = \left(\rho c_p\right)_{S,1} \frac{\Delta T_{S,1}}{\Delta \tau} + \frac{c_p \dot{m}}{2\delta\, \Delta\eta} \left(3T_{S,1} + T_{S-2,1} - 4T_{S-1,1}\right) \tag{C26}$$

For station (m = 1, 1 < n < L), equations (9) and (26) combine to give

$$\frac{1}{x_b^2 \Delta\xi^2} \left[\left(\frac{h_3 k_\xi}{h_1}\right)_{1,n+\frac{1}{2}} \left(T_{1,n+1} - T_{1,n}\right) - \left(\frac{h_3 k_\xi}{h_1}\right)_{1,n-\frac{1}{2}} \left(T_{1,n} - T_{1,n-1}\right)\right]$$

$$+ \frac{1}{3\delta^2 \Delta\eta^2} \left\{9\left(h_1 h_3 k_\eta\right)_{3/2,n} \left(T_{2,n} - T_{1,n}\right) - \left(h_1 h_3 k_\eta\right)_{5/2,n} \left(T_{3,n} - T_{2,n}\right)\right.$$

$$\left. - \left(8 h_1 h_3\, \Delta\eta\delta\right)_{1,n} \left[\rho'' c_p'' t'' \frac{\Delta T_{1,n}}{\Delta \tau} + \sigma\epsilon'' \left(T_{1,n}^4 - T_B^4\right)\right]\right\} = \left(h_1 h_3 \rho c_p\right)_{1,n} \frac{\Delta T_{1,n}}{\Delta \tau} \tag{C27}$$

For station (m = S, 1 < n < L), combining equations (9) and (20) yields:

$$\frac{1}{3\delta^2 \Delta\eta^2} \left[\left(h_1 h_3 k_\eta\right)_{S-\frac{3}{2},n} \left(T_{S-1,n} - T_{S-2,n}\right) - 9\left(h_1 h_3 k_\eta\right)_{S-\frac{1}{2},n} \left(T_{S,n} - T_{S-1,n}\right)\right.$$

$$\left. + 8\left(h_1 h_3 \delta\, \Delta\eta\right)_{S,n} \left(q_{net}\right)_{S,n}\right] + \frac{1}{x_b^2 \Delta\xi^2} \left[\left(\frac{h_3 k_\xi}{h_1}\right)_{S,n+\frac{1}{2}} \left(T_{S,n+1} - T_{S,n}\right)\right.$$

(Equation continued on next page)

$$- \left(\frac{h_3 k_\xi}{h_1}\right)_{S,n-\frac{1}{2}} \left(T_{S,n} - T_{S,n-1}\right)\Bigg] - \frac{1}{2x_b\,\Delta\xi}\left\{\left(\frac{h_3 k_\xi \eta A}{h_1 \delta}\right)_{S,n+\frac{1}{2}}\left[\left(\frac{\delta}{k_\eta}\right)_{S,n+1}\left(q_{net}\right)_{S,n+1}\right.\right.$$

$$\left.\left. + \left(\frac{\delta}{k_\eta}\right)_{S,n}\left(q_{net}\right)_{S,n}\right] - \left(\frac{h_3 k_\xi \eta A}{h_1 \delta}\right)_{S,n-\frac{1}{2}}\left[\left(\frac{\delta q_{net}}{k_\eta}\right)_{S,n} + \left(\frac{\delta q_{net}}{k_\eta}\right)_{S,n-1}\right]\right\}$$

$$+ \frac{1}{3\,\Delta\eta^2}\left(\frac{A}{\delta}\right)_{S,n}\left[\left(\frac{h_3 k_\xi \eta A}{h_1 \delta}\right)_{S-\frac{3}{2},n}\left(T_{S-1,n} - T_{S-2,n}\right)\right.$$

$$\left. - 9\left(\frac{h_3 k_\xi \eta A}{h_1 \delta}\right)_{S-\frac{1}{2},n}\left(T_{S,n} - T_{S-1,n}\right) + 8\left(\frac{h_3 k_\xi \eta A\,\Delta\eta q_{net}}{k_\eta h_1}\right)_{S,n}\right]$$

$$- \left(\frac{A}{4\delta x_b\,\Delta\eta\,\Delta\xi}\right)_{S,n}\left[3\left(\frac{h_3 k_\xi}{h_1}\right)_{S,n}\left(T_{S,n+1} - T_{S,n-1}\right)\right.$$

$$\left. - 4\left(\frac{h_3 k_\xi}{h_1}\right)_{S-1,n}\left(T_{S-1,n+1} - T_{S-1,n-1}\right) + \left(\frac{h_3 k_\xi}{h_1}\right)_{S-2,n}\left(T_{S-2,n+1} - T_{S-2,n-1}\right)\right]$$

$$= \left(h_1 h_3 \rho c_p\right)_{S,n}\left[\frac{\Delta T_{S,n}}{\Delta\tau} + \left(\frac{\eta \dot{m}}{2\delta\rho\,\Delta\eta}\right)_{S,n}\left(3T_{S,n} - 4T_{S-1,n} + T_{S-2,n}\right)\right] \tag{C28}$$

For station (m = 1, n = L), combining equations (9), (22), and (23) gives

$$\frac{1}{3x_b^2\Delta\xi}\left\{\left(\frac{h_3 k_\xi}{h_1}\right)_{1,L-\frac{3}{2}}\left(\frac{T_{1,L-1} - T_{1,L-2}}{\Delta\xi}\right) - 9\left(\frac{h_3 k_\xi}{h_1}\right)_{1,L-\frac{1}{2}}\left(\frac{T_{1,L} - T_{1,L-1}}{\Delta\xi}\right)\right.$$

$$\left. - 8\left(h_3 x_b\right)_{1,L}\left[t' c_p' \rho' \frac{\Delta T_{1,L}}{\Delta\tau} + \sigma\epsilon'\left(T_{1,L}^4 - T_B^4\right)\right]\right\} + \frac{1}{3\delta^2\Delta\eta}\left\{-\left(h_1 h_3 k_\eta\right)_{5/2,L}\left(\frac{T_{3,L} - T_{2,L}}{\Delta\eta}\right)\right.$$

(Equation continued on next page)

$$+ 9\left(h_1 h_3 k_\eta\right)_{3/2,L}\left(\frac{T_{2,L} - T_{1,L}}{\Delta\eta}\right) - 8\left(h_1 h_3 \delta\right)_{1,L}\left[\rho'' c_p'' t'' \frac{\Delta T_{1,L}}{\Delta\tau} + \sigma\epsilon''\left(T_{1,L}^4 - T_B^4\right)\right]\Bigg\}$$

$$= \left(h_1 h_3 \rho c_p\right)_{1,L} \frac{\Delta T_{1,L}}{\Delta\tau} \qquad \text{(C29)}$$

For stations ($1 < m < S$, $n = L$), equations (9) and (23) yield

$$\frac{1}{3x_b\,\Delta\xi}\Bigg\{- 9\left(\frac{h_3 k_\xi}{h_1}\right)_{m,L-\frac{1}{2}}\Bigg[\frac{\left(T_{m,L} - T_{m,L-1}\right)}{x_b\,\Delta\xi} + \left(\frac{\eta A}{4\,\Delta\eta\delta}\right)_{m,L-\frac{1}{2}}\left(T_{m+1,L} - T_{m-1,L}\right.$$

$$\left. + T_{m+1,L-1} - T_{m-1,L-1}\right)\Bigg] + \left(\frac{h_3 k_\xi}{h_1}\right)_{m,L-\frac{3}{2}}\Bigg[\frac{\left(T_{m,L-1} - T_{m,L-2}\right)}{x_b\,\Delta\xi}$$

$$- \left(\frac{\eta A}{4\delta\,\Delta\eta}\right)_{m,L-\frac{3}{2}}\left(T_{m+1,L-1} - T_{m-1,L-1} + T_{m+1,L-2} - T_{m-1,L-2}\right)\Bigg]$$

$$- 8\left(h_3\right)_{m,L}\left[\rho' c_p' t' \frac{\Delta T_{m,L}}{\Delta\tau} + \sigma\epsilon'\left(T_{m,L}^4 - T_B^4\right)\right]\Bigg\} - \left(\frac{\eta A k_\xi}{4x_b\delta\,\Delta\eta\,\Delta\xi}\right)_{m,L}\Bigg[\left(\frac{h_3}{h_1}\right)_{m+1,L}\left(3T_{m+1,L}\right.$$

$$\left. - 4T_{m+1,L-1} + T_{m+1,L-2}\right) - \left(\frac{h_3}{h_1}\right)_{m-1,L}\left(3T_{m-1,L} - 4T_{m-1,L-1} + T_{m-1,L-2}\right)\Bigg]$$

$$+ \left(\frac{\eta A k_\xi}{\delta^2 \Delta\eta^2}\right)_{m,L}\Bigg[\left(\frac{h_3 \eta A}{h_1}\right)_{m+\frac{1}{2},L}\left(T_{m+1,L} - T_{m,L}\right) - \left(\frac{h_3 \eta A}{h_1}\right)_{m-\frac{1}{2},L}\left(T_{m,L} - T_{m-1,L}\right)\Bigg]$$

$$+ \left(\frac{1}{\delta^2 \Delta\eta^2}\right)_{m,L}\Bigg[\left(h_1 h_3 k_\eta\right)_{m+\frac{1}{2},L}\left(T_{m+1,L} - T_{m,L}\right) - \left(h_1 h_3 k_\eta\right)_{m-\frac{1}{2},L}\left(T_{m,L} - T_{m-1,L}\right)\Bigg]$$

$$= \left(h_1 h_3 \rho c_p\right)_{m,L}\Bigg[\frac{\Delta T_{m,L}}{\Delta\tau} + \left(\frac{\dot{m}\eta}{\delta\rho}\right)_{m,L}\left(\frac{T_{m+1,L} - T_{m-1,L}}{2\,\Delta\eta}\right)\Bigg]$$

(C30)

For station (m = S, n = L), equations (9), (20), and (23) are combined to yield

$$\frac{1}{3x_b\,\Delta\xi}\Bigg(-9\left(\frac{h_3k_\xi}{h_1}\right)_{S,L-\frac{1}{2}}\left\{\left(\frac{T_{S,L}-T_{S,L-1}}{x_b\,\Delta\xi}\right)-\left(\frac{A}{2\delta}\right)_{S,L-\frac{1}{2}}\left[\left(\frac{\delta q_{net}}{k_\eta}\right)_{S,L}+\left(\frac{\delta q_{net}}{k_\eta}\right)_{S,L-1}\right]\right\}$$

$$+\left(\frac{h_3k_\xi}{h_1}\right)_{S,L-\frac{3}{2}}\left\{\left(\frac{T_{S,L-1}-T_{S,L-2}}{x_b\,\Delta\xi}\right)-\left(\frac{A}{2\delta}\right)_{S,L-\frac{3}{2}}\left[\left(\frac{\delta q_{net}}{k_\eta}\right)_{S,L-1}+\left(\frac{\delta q_{net}}{k_\eta}\right)_{S,L-2}\right]\right\}$$

$$-8(h_3)_{S,L}\left[\rho' c_p' t'\,\frac{\Delta T_{S,L}}{\Delta\tau}+\sigma\epsilon'\left(T_{S,L}^4-T_B^4\right)\right]\Bigg)$$

$$-\left(\frac{A}{3\delta\,\Delta\eta}\right)_{S,L}\Bigg\{-9\left(\frac{h_3k_\xi}{h_1}\right)_{S-\frac{1}{2},L}\left[\left(\frac{3T_{S,L}-4T_{S,L-1}+T_{S,L-2}+3T_{S-1,L}-4T_{S-1,L-1}+T_{S-1,L-2}}{4x_b\,\Delta\xi}\right)\right.$$

$$\left.-\left(\frac{\eta A}{\delta\,\Delta\eta}\right)_{S-\frac{1}{2},L}\left(T_{S,L}-T_{S-1,L}\right)\right]+\left(\frac{h_3k_\xi}{h_1}\right)_{S-\frac{3}{2},L}\left[\left(\frac{3T_{S-2,L}-4T_{S-2,L-1}+T_{S-2,L-2}}{4x_b\,\Delta\xi}\right)\right.$$

$$\left.+\left(\frac{3T_{S-1,L}-4T_{S-1,L-1}+T_{S-1,L-2}}{4x_b\,\Delta\xi}\right)-\left(\frac{\eta A}{\delta\,\Delta\eta}\right)_{S-\frac{3}{2},L}\left(T_{S-1,L}-T_{S-2,L}\right)\right]$$

$$-8(h_3)_{S,L}\left[\rho' c_p' t''\,\frac{\Delta T_{S,L}}{\Delta\tau}+\sigma\epsilon'\left(T_{S,L}^4-T_B^4\right)\right]\Bigg\}$$

$$+\left(\frac{1}{3\,\Delta\eta^2\delta^2}\right)_{S,L}\Bigg[\left(h_1h_3k_\eta\right)_{S-\frac{3}{2},L}\left(T_{S-1,L}-T_{S-2,L}\right)-9\left(h_1h_3k_\eta\right)_{S-\frac{1}{2},L}\left(T_{S,L}-T_{S-1,L}\right)$$

$$+8\,\Delta\eta\left(h_1h_3\delta q_{net}\right)_{S,L}\Bigg]=\left(h_1h_3\rho c_p\right)_{S,L}\left[\frac{\Delta T_{S,L}}{\Delta\tau}+\frac{\dot m}{2\delta\,\Delta\eta\rho}\left(3T_{S,L}-4T_{S-1,L}+T_{S-2,L}\right)\right] \qquad (C31)$$

APPENDIX D

DERIVATION OF EXACT SOLUTION

The governing differential equation for the steady-state temperature distribution in an internally insulated, thick-walled, hollow hemisphere shown schematically in figure 4 is

$$\frac{1}{r^2}\frac{\partial}{\partial r}\left(r^2\frac{\partial T}{\partial r}\right)+\frac{1}{r^2\sin\theta}\frac{\partial}{\partial\theta}\left(\sin\theta\frac{\partial T}{\partial\theta}\right)=0 \tag{D1}$$

The boundary conditions are

$$\left.\frac{\partial T}{\partial\theta}\right|_{\theta=0,\pi/2}=\left.\frac{\partial T}{\partial r}\right|_{r=R}=0 \tag{D2}$$

and

$$T(R+\delta,\theta)=T_o(1+\cos^2\theta) \tag{D3}$$

The general solution to equation (D1) by the method of separation of variables is

$$T(r,\theta)=\left(D_0-\frac{C_0}{r}\right)\left[B_0\ln\left(\tan\frac{\theta}{2}\right)+A_0\right]+\sum_{n=1}^{\infty}A_nP_n(\cos\theta)\left[C_nr^n+D_nr^{-(n+1)}\right] \tag{D4}$$

where A_0, B_0, C_0, D_0, A_n, C_n, and D_n are constants of integration and $P_n(\cos\theta)$ is the Legendre polynomial.

When the boundary conditions, equations (D2) and (D3), are used to evaluate the coefficients in equation (D4), the solution to equation (D1) is

$$T(r,\theta)=\frac{4}{3}T_o+\frac{T_o(3\cos^2\theta-1)\left(r^2+\frac{2}{3}R^5r^{-3}\right)}{3\left[(R+\delta)^2+\frac{2}{3}(R+\delta)^{-3}R^5\right]} \tag{D5}$$

REFERENCES

1. Peterson, W. D.; and Spanier, J.: HOT-2: A Two-Dimensional Transient Heat Conduction Program for the CDC-6600. WAPD-TM-669, U.S. At. Energy Comm., June 1967.

2. McClure, John A.: TOODEE – A Two-Dimensional, Time-Dependent Heat Conduction Program. AEC Res. and Develop. Rep. IDO-17227, U.S. At. Energy Comm., April 1967.

3. Friedman, H. A.; and McFarland, B. L.: Two-Dimensional Transient Ablation and Heat Conduction Analysis for Multimaterial Thrust Chamber Walls. J. Spacecraft Rockets, vol. 5, no. 7, July 1968, pp. 753-761.

4. McCuen, Peter A.; Schaefer, John W.; Lundberg, Raymond E.; and Kendall, Robert M.: A Study of Solid-Propellant Rocket Motor Exposed Materials Behavior. AFRPL-TR-65-33, U.S. Air Force, Feb. 26, 1965.

5. Popper, L. A.; Toong, T. Y.; and Sutton, G. W.: Three-Dimensional Ablation Considering Shape Changes and Internal Heat Condition. AIAA Paper No. 70-199, Jan. 1970.

6. Moyer, Carl B.; Anderson, Larry W.; and Dahm, Thomas J.: A Coupled Computer Code for the Transient Thermal Response and Ablation of Non-Charring Heat Shields and Nose Tips. NASA CR-1630, 1970.

7. Thornton, William A.; and Schmit, Lucien A., Jr.: The Structural Synthesis of an Ablating Thermostructural Panel. NASA CR-1215, 1968.

8. Swann, Robert T.; Pittman, Claud M.; and Smith, James C.: One-Dimensional Numerical Analysis of the Transient Response of Thermal Protection Systems. NASA TN D-2976, 1965.

9. Scala, Sinclaire M.; and Gilbert, Leon M.: Sublimation of Graphite at Hypersonic Speeds. AIAA J., vol. 3, no. 9, Sept. 1965, pp. 1635-1644.

10. McCarthy, J. F., Jr.; and Hanley, G. M.: Earth Entry at Hyperbolic Velocities. AIAA Paper No. 68-153, Jan. 1968.

11. Lees, Lester: Laminar Heat Transfer Over Blunt-Nosed Bodies at Hypersonic Flight Speeds. Jet Propulsion, vol. 26, no. 4, Apr. 1956, pp. 259-269, 274.

12. Gavril, Bruce D.; and Lane, Frank: Finite Difference Equations and Their Solution for the Transient Temperature Distribution in Composite, Anisotropic, Generalized Bodies of Revolution. Tech. Rep. No. 230 (Contract No. NOrd 18053), Gen. Appl. Sci. Lab., Inc., May 26, 1961.

13. Brooks, William A., Jr.: Temperature and Thermal-Stress Distributions in Some Structural Elements Heated at a Constant Rate. NACA TN 4306, 1958.

14. Howell, Robert R.: An Experimental Study of the Behavior of Spheres Ablating Under Constant Aerodynamic Conditions. NASA TN D-1635, 1963.

15. Brewer, William D.: Ablative Material Performance in High Radiative Heat Flux Environment Produced by a Carbon Dioxide Laser. AIAA Paper No. 70-864, June-July 1970.

NASA-Langley, 1971 —— 33 L-7474

NATIONAL AERONAUTICS AND SPACE ADMINISTRATION
WASHINGTON, D.C. 20546

OFFICIAL BUSINESS
PENALTY FOR PRIVATE USE $300

FIRST CLASS MAIL

POSTAGE AND FEES PAID
NATIONAL AERONAUTICS AND
SPACE ADMINISTRATION

10U 001 58 51 3DS 71147 00903
AIR FORCE WEAPONS LABORATORY /WLOL/
KIRTLAND AFB, NEW MEXICO 87117

ATT E. LOU BOWMAN, CHIEF, TECH. LIBRARY

POSTMASTER: If Undeliverable (Section 158 Postal Manual) Do Not Return

"The aeronautical and space activities of the United States shall be conducted so as to contribute . . . to the expansion of human knowledge of phenomena in the atmosphere and space. The Administration shall provide for the widest practicable and appropriate dissemination of information concerning its activities and the results thereof."

—NATIONAL AERONAUTICS AND SPACE ACT OF 1958

NASA SCIENTIFIC AND TECHNICAL PUBLICATIONS

TECHNICAL REPORTS: Scientific and technical information considered important, complete, and a lasting contribution to existing knowledge.

TECHNICAL NOTES: Information less broad in scope but nevertheless of importance as a contribution to existing knowledge.

TECHNICAL MEMORANDUMS: Information receiving limited distribution because of preliminary data, security classification, or other reasons.

CONTRACTOR REPORTS: Scientific and technical information generated under a NASA contract or grant and considered an important contribution to existing knowledge.

TECHNICAL TRANSLATIONS: Information published in a foreign language considered to merit NASA distribution in English.

SPECIAL PUBLICATIONS: Information derived from or of value to NASA activities. Publications include conference proceedings, monographs, data compilations, handbooks, sourcebooks, and special bibliographies.

TECHNOLOGY UTILIZATION PUBLICATIONS: Information on technology used by NASA that may be of particular interest in commercial and other non-aerospace applications. Publications include Tech Briefs, Technology Utilization Reports and Technology Surveys.

Details on the availability of these publications may be obtained from:

SCIENTIFIC AND TECHNICAL INFORMATION OFFICE

NATIONAL AERONAUTICS AND SPACE ADMINISTRATION

Washington, D.C. 20546